

Massive, red galaxies in a hierarchical universe-I Counts of Extremely Red Objects and basic properties

V. Gonzalez-Perez¹, C. M. Baugh², C.G.Lacey², C. Almeida².

¹*Institut de Ciències de l’Espai (CSIC/IEEC), F. de Ciències, Torre C5 Par 2a, UAB, Bellaterra, 08193 Barcelona, Spain*

²*Institute for Computational Cosmology, Department of Physics, University of Durham, South Road, Durham, DH1 3LE, UK.*

3 November 2018

ABSTRACT

We present predictions for the abundance and nature of Extremely Red Objects (EROs) in the Λ cold dark matter model. EROs are red, massive galaxies observed at $z \geq 1$ and their numbers and properties pose a challenge to hierarchical galaxy formation models. We compare the predictions from two published models, one of which invokes a “superwind” to regulate star formation in massive haloes and the other which suppresses gas cooling in haloes through “radio-mode” AGN feedback. The superwind model underestimates the number counts of EROs by an order of magnitude, whereas the radio-mode AGN feedback model gives excellent agreement with the number counts and redshift distribution of EROs. In the AGN feedback model the ERO population is dominated by old, passively evolving galaxies, whereas observations favour an equal split between old galaxies and dusty starbursts. Also, the model predicts a more extended redshift distribution of passive galaxies than is observed. These comparisons suggest that star formation may be quenched too efficiently in this model.

1 INTRODUCTION

Advances in near-infrared detector technology have made possible the identification of large samples of massive, red galaxies at redshifts when the universe was less than half its current age (e.g. Elston et al. 1988; Thompson et al. 1999; Daddi et al. 2000; McCarthy et al. 2001; Cimatti et al. 2002a; Smith et al. 2002; Simpson et al. 2006; Conselice et al. 2008). These objects, according to estimates based on their K-band fluxes, have stellar masses comparable to the most massive galaxies in place today (Cimatti et al. 2004; Glazebrook et al. 2004). Extremely red objects (EROs) are among these galaxies. Their extremely red optical-near infrared colours, indicate either a star-forming galaxy with heavy obscuration or an aged stellar population with little recent star formation (Pozzetti & Mannucci 2000; Smail et al. 2002; Cimatti et al. 2003). In the latter case, the implied age of the stellar population is uncomfortably close to the age of the Universe at the redshift of observation (Cimatti et al. 2002a; Smith et al. 2002).

At face value either ERO scenario might appear difficult to reconcile with a universe in which structure in the dark matter grows in a bottom-up sequence, with smaller haloes merging to make more massive haloes. If the universe is assumed to be populated by low mass dark matter haloes at high redshift, and, as is traditionally argued, these haloes are ineffective at making galaxies due to feedback from supernova explosions, how can the stars in EROs have formed by the high redshifts suggested by observations? Where are the deep potential wells in which enough cold gas has ac-

cumulated for luminous, dusty starbursts to take place? In practice, two effects act to make it possible for the stars in massive objects to form at high redshift in a cold dark matter model. First, the range of halo masses collapsing at a given redshift is actually very broad in the CDM model, due to the shape of the power spectrum of density fluctuations (see e.g. Mo & White 2002). Second, the progenitors of massive haloes form at an earlier epoch than similar mass progenitors which end up in less extreme mass haloes. This in turn means that these progenitors can start to form stars earlier (see Neistein et al. 2006; de Lucia et al. 2006).

Earlier generations of hierarchical galaxy formation models did indeed fail to match the observed abundance of EROs, by around an order of magnitude (Smith et al. 2002; Firth et al. 2002; Roche et al. 2002) and predicted an ERO redshift distribution that was too shallow (Cimatti et al. 2002b; Somerville et al. 2004). This initial failure led to attempts to resurrect the monolithic collapse scenario for massive galaxy formation, in which all the stars in a galaxy form at the same epoch (Eggen et al. 1962). Pure luminosity evolution (PLE) models, simple parametric functions which are meant to describe the brightness of a stellar population as a function of time, can be adjusted to give reasonable matches to the number counts and redshift distributions of EROs (e.g. Daddi et al. 2000). However, such an approach soon falls apart when applied to more than one type of galaxy. Kitzbichler & White (2006) demonstrated that PLE models that give mass-to-light ratios consistent with the red sequence of galaxies found in clusters have the drawback that they overpredict the number counts of magnitude-limited samples at faint magnitudes.

Recently there has been much development in the modelling of the formation of massive galaxies. This activity was primarily directed at solving the problem of matching the bright end of the local galaxy luminosity function, but also has implications for the abundance of massive galaxies at high redshift. Typically, hierarchical models, based on the current best fitting values of the cosmological parameters, produce too many massive galaxies at the present day unless some physical process is invoked to restrict gas cooling in massive haloes (see e.g. Benson et al. 2003, for a review of plausible mechanisms). The most promising candidates are the heating of gas in quasi-hydrostatically cooling haloes in which “radio mode” AGN feedback is considered to be effective (Bower et al. 2006; Croton et al. 2006; Kang et al. 2006; Cattaneo et al. 2006; Lagos et al. 2008), the ejection of gas from intermediate mass haloes in a wind, which could be driven by supernovae (e.g. Benson et al. 2003; Baugh et al. 2005) or “quasar mode” feedback which follows accretion of cold gas driven by a galaxy merger or the collapse of an unstable disk (Granato et al. 2004; Hopkins et al. 2006; Menci et al. 2006). Recent models (see Sijacki et al. 2007; Monaco et al. 2007; Somerville et al. 2008) incorporate both the radio and quasar modes of feedback and their corresponding impact on star formation in the host galaxy.

Several authors have gone back to the problem of the abundance of massive galaxies following the recent improvements in the theoretical models. There are several conditions to bear in mind when assessing the merits of a model which claims to reproduce a given dataset, such as the number counts of EROs: (i) Does the model attempt to follow the full galaxy population or just some component of it, such as spheroids? (ii) Does the model follow the galaxy population to the present day? Can the same model, which successfully matches observations at high redshift, also reproduce local data? (iii) How is the comparison with observations carried out? Is it direct, relying on photometric selection of galaxies or is it indirect, using quantities which are not directly observed, such as stellar mass, to compare galaxies?

Nagamine et al. (2005) compared calculations made with Eulerian and Lagrangian gas-dynamics codes and found that, with their choice of “sub-grid” physics to describe baryonic processes, they did not have a problem in reproducing the number of massive galaxies seen at high redshift. However, producing the observed number of galaxies with red colours proved to be more challenging. Nagamine et al. found they could obtain the correct number of EROs if they assumed all EROs to be heavily extinguished starbursts (applying by hand an extinction equivalent to $E(B - V) = 0.4$ to each galaxy), and without any galaxies which displayed the colours of old, passively evolving stellar populations. Observationally, passive galaxies and dusty starbursts contribute roughly equally to the counts of EROs (e.g. Mannucci 2002; Cimatti et al. 2002a).

Models in which radio mode AGN feedback suppresses gas cooling in massive haloes seem to have taken significant steps towards solving the massive red galaxy problem. Kitzbichler & White (2007) studied the abundance of massive galaxies in the semi-analytical model of de Lucia & Blaizot (2007). This model actually overpredicts the number counts of galaxies faintwards of $K_{AB} \sim 20$ and predicts more extended redshift distributions than are observed, which means that the model has *too much*

star formation at high redshift. Kang et al. (2006), on the other hand, claim to reproduce the number of EROs with $(R - K) > 5$, but not the number defined by redder cuts. The Kang et al. model, however, overpredicts the number of bright galaxies in the K-band luminosity function today. Another problem is that this model predicts a lower median redshift for K-selected galaxies than is observed.

Alternative models have been proposed in which feedback in massive haloes occurs during the quasar mode of mass accretion onto black holes, i.e. the QSO phase of an AGN. The QSO episode is assumed to be triggered by a galaxy interaction or merger, or the dynamical instability of a galactic disk. As a result cold gas moves towards the centre of the galaxy, and some fraction is added to a supermassive black hole via an accretion disk. The QSO activity peaks at high redshift, when the merger rate is higher and when larger reservoirs of cold gas are in place. At the onset of the QSO phase, the remaining gas in the galaxy is blasted out and the star formation terminates (Silk & Rees 1998). This quasar mode feedback is distinct from the radio mode mentioned above which acts predominantly at later times or in haloes which are massive enough for quasi-static hot atmospheres to form. In the radio mode, the black hole is fuelled by the accretion of gas in a cooling flow. Quasar mode feedback has been implemented into several semi-analytical models. Granato et al. (2004) argued that QSO feedback eventually truncates star formation, causing the stellar population of the galaxy to age, resulting in EROs. However, these authors were only able to track galactic spheroids in their model. Fontanot et al. (2007) consider a semi-analytical code with a new cooling model which is able to match the counts but not the redshifts of sub-mm galaxies using a standard stellar initial mass function. However, their preferred model overpredicts the local abundance of bright galaxies by at least an order of magnitude. Perhaps the most successful model of this type to date is that of Menci et al. (2006) which is able to reproduce the counts and redshift distribution of EROs, along with the rest-frame B-band luminosity function over the interval $0.4 \leq z \leq 3.5$. With QSO feedback models, the problem of overcooling in massive haloes at low redshifts remains, unless the gas expelled in the QSO feedback episode is prevented from being recaptured. As mentioned above, recent models have incorporated both radio and quasar modes of feedback (Sijacki et al. 2007; Somerville et al. 2008).

In this paper we examine the predictions for EROs from two published semi-analytical models, Baugh et al. (2005) and Bower et al. (2006). The models invoke different mechanisms to suppress star formation in massive galaxies. In Baugh et al., a wind ejects gas from low and intermediate mass haloes, with the mass ejection rate tied to the star formation rate. Due to the ejection of gas, the baryon fraction in massive haloes is therefore lower than the universal baryon fraction, reducing the cooling rate. The Bower et al. model invokes radio-mode AGN feedback to suppress gas cooling in massive haloes. The parameters in both models are set by the requirement that they reproduce a subset of local galaxy observations. Almeida et al. (2008) investigated the predictions of these models for the abundance of luminous red galaxies (Eisenstein et al. 2001). Here, we extend this comparison to much higher redshifts by looking at the predictions for EROs. This is the first in a series of three papers. In this paper we look at the number counts, redshift

distributions and other basic properties of EROs in the models; in the second paper we study the clustering of EROs and their descendants and in the third paper we compare the implications of different selections for red galaxies. This paper is organized as follows. In Section 2, we summarize the two galaxy formation models used to study the EROs population. The predictions for the abundance and redshift distribution of EROs are given in Section 3. The nature of EROs in the model is discussed in Section 4 and their basic properties are presented in Section 5. Our conclusions are presented in Section 6.

The bands used here correspond to the R band from SUBARU, centred at $0.65 \mu\text{m}$, and the K band from UKIRT, with a central wavelength of $2.2 \mu\text{m}$. All magnitudes used in this paper are on the Vega system, unless otherwise specified. The cosmological parameters of the models are given in Section 2.

2 GALAXY FORMATION MODEL

We predict the abundance and properties of EROs in a ΛCDM universe using the `GALFORM` semi-analytical galaxy formation code developed by Cole et al. (2000), and extended by Benson et al. (2003) and Bower et al. (2006). Semi-analytical models use simple, physically motivated recipes and rules to follow the fate of baryons in a universe in which structures grow hierarchically through gravitational instability (see Baugh 2006, for an introduction to hierarchical galaxy formation models).

In this paper we focus our attention on two published models, Baugh et al. (2005) and Bower et al. (2006). The parameters of these models were fixed with reference to a subset of the available observations of galaxies, mostly at low redshift. In this paper we extract predictions for the number and nature of ERO galaxies without adjusting the values of any of the model parameters. Although none of the datasets used to set the model parameters explicitly referred to EROs, one of our priorities in adjusting parameter values is to obtain as good a match as possible to the bright end of the local field galaxy luminosity function. Observationally, the bright end of the luminosity function tends to be dominated by galaxies with red colours and passively evolving stellar populations (e.g. Norberg et al. 2002). Hence by reproducing the observed luminosity function, the models have approximately the right number of bright red galaxies today. By testing the predictions for EROs, we are therefore probing the evolution of the bright red galaxy population in the models to $z > 1$.

In addition to reproducing local galaxy data, the models have some notable successes at high redshift. The Bower et al. model matches the inferred evolution of the stellar mass function to $z = 4.5$. The Baugh et al. model matches the number and redshift distribution of galaxies detected by their emission at sub-millimetre wavelengths (see also the predictions presented by Lacey et al. 2008), the luminosity function of Lyman break galaxies and the abundance and clustering of Lyman-alpha emitters (Le Delliou et al. 2005, 2006; Orsi et al. 2008).

We now recap some of the key features of the models for the study presented in this paper and draw attention to places where the two models differ. A similar com-

parison of the two models can be found in Almeida et al. (2007, 2008). For a comprehensive inventory of the ingredients of the models, we refer the reader to the original papers (see also Lacey et al. 2008, for a recap of the ingredients of Baugh et al.).

- *Cosmology.* Baugh et al. use the canonical (ΛCDM) parameters: matter density, $\Omega_0 = 0.3$, cosmological constant, $\Lambda_0 = 0.7$, baryon density, $\Omega_b = 0.04$, a normalization of density fluctuations given by $\sigma_8 = 0.93$ and a Hubble constant $h = 0.7$ in units of $100 \text{ km s}^{-1} \text{ Mpc}^{-1}$. Bower et al. adopt the cosmological parameters of the Millennium Simulation (Springel et al. 2005), which are in better agreement with recent constraints from measurements of the cosmic microwave background radiation and large scale galaxy clustering (e.g. Sánchez et al. 2006): $\Omega_0 = 0.25$, $\Lambda_0 = 0.75$, $\Omega_b = 0.045$, $\sigma_8 = 0.9$ and $h = 0.73$.

- *Dark matter halo merger trees.* The Baugh et al. model employs merger trees generated using the Monte Carlo algorithm introduced by Cole et al. (2000). The Bower et al. model uses halo merger histories extracted from the Millennium Simulation (Springel et al. 2005). These two approaches have been shown to yield similar results for galaxies brighter than a limiting faint magnitude which is determined by the mass resolution of the N-body trees (Helly et al. 2003). In the case of the Millennium merger trees, this limit is several magnitudes fainter than L_* and so will have little consequence for the study of EROs, which are much brighter. We compute number counts in the Baugh et al. model by growing merger histories for representative grids of halo masses laid down at a range of output redshifts, rather than outputting the branches of one set of trees grown from $z = 0$. In this way, we avoid any biases in the progenitor distribution which may develop over large lookback times. Recently, a more accurate Monte Carlo prescription for generating merger histories has been developed and it would be instructive to re-run the Baugh et al. model with these modified trees (Parkinson et al. 2008).

- *Feedback processes.* Both models regulate star formation by the injection of energy from supernova explosions into the cold gas reservoir. In Baugh et al., there are two consequences of this energy injection which are parameterized in different ways and which also differ in the fate of the reheated gas. In the “standard” mode of supernova feedback, cold gas is heated and ejected from the galactic disk. In Baugh et al., this gas is not allowed to recool until a new halo has formed (as signalled by a doubling of the halo mass), whereupon this reheated gas is incorporated into the hot gas atmosphere of the new halo. In the “superwind” mode of feedback, reheated gas is expelled completely from the halo, and in this particular implementation is never allowed to recool. These two modes of supernova feedback can operate side-by-side in a given halo, with relative strengths determined by the parameter values chosen (see Lacey et al. 2008). Benson et al. (2003) give a more detailed discussion of these modes of feedback. The superwind suppresses the formation of bright galaxies in massive haloes. It achieves this by ejecting gas from the progenitors of the massive halo, so that the hot gas reservoir is depleted, and the massive halo effectively has a baryon fraction that is lower than the universal value. One concern is that the parameters in the feedback recipes are chosen without reference to the total

amount of energy available from supernova explosions. Once a reasonable match to the bright end of the luminosity function has been obtained, the implied efficiency with which the energy released by supernovae must couple to heating the intergalactic medium is uncomfortably high. Bower et al. also invoke “standard” supernovae feedback, though with very different parameters values than those used in Baugh et al.. This is due in part to a modification in the handling of the gas reheated by supernova feedback. Rather than being placed in limbo until a new halo forms, the reheated gas is incorporated into the hot halo after some number of halo dynamical times. Hence gas can recool more rapidly in Bower et al., which explains why the standard supernova feedback parameters are set to values which correspond to stronger feedback than in Baugh et al. In Bower et al., there is no superwind feedback. The formation of bright galaxies is suppressed by staunching the cooling flow in massive haloes using “radio-mode” AGN feedback. This is achieved by the injection of energy into the quasistatic hot halo, which is generated by the accretion of matter onto a central supermassive black hole (see Malbon et al. 2007, for a description of the model of black hole growth).

- *Star formation.*: In the models, stars can form quiescently in galactic disks or in bursts. The two models adopt different redshift dependencies for the time-scale for quiescent star formation. Baugh et al. adopt a fixed time-scale whereas in Bower et al., the time-scale depends on the dynamical time. In both models, mergers can trigger starbursts, though the conditions for a burst to occur are different. Baugh et al. include only bursts triggered by galaxy mergers, whereas Bower et al. also consider bursts which result from disks becoming dynamically unstable to the formation of a bar.

- *Stellar Initial Mass Function (IMF).* Both models adopt the Kennicutt (1983) IMF for quiescent star formation. Bower et al. also use this IMF in starbursts, whereas Baugh et al. invoke a top-heavy IMF. This choice, though controversial, is the key to the success of Baugh et al. in reproducing sub-mm galaxies number counts and also the metallicity of the intracluster medium (Nagashima et al. 2005). The yield of metals and the fraction of gas recycled in star formation are determined by the choice of IMF.

Finally in this section, we discuss one element which the models have in common, the treatment of dust extinction, which is important for our purposes as it has an impact on galaxy colours. Both models employ an extension of the dust extinction calculation introduced by Cole et al. (2000). *GALFORM* makes a self-consistent calculation of the dust optical depth of a galaxy, computing the gas mass and metallicity based on a chemical evolution model and making a prediction for the scale length of the disk and bulge components. The size calculation is also explained by Cole et al. (see Almeida et al. 2007 for a test of this calculation for spheroids). In brief, for the disk component, the model assumes the conservation of angular momentum of the gas. The size of spheroids is calculated following a merger by considering the conservation of energy and the application of the virial theorem. The size of the disk and bulge components also takes into account the gravity of the baryons and the dark matter. The stars are assumed to be mixed in with the dust, with the possibility that the two components may

have different scale heights. The dust is assumed to have the properties consistent with the extinction law observed in the Milky Way. An inclination angle is assigned at random to the galactic disk. The dust extinction is then computed using the results of radiative transfer calculations carried out by Ferrara et al. (1999). This model is a significant improvement over calculations using foreground screens, in which a slab of dust is assumed to be along the line of sight to the stars and an empirical estimate is made of the optical depth.

The extension we apply to the dust extinction model of Cole et al. is to assume that some fraction of the dust is in the form of dense molecular clouds where the stars form (see Baugh et al. 2005). This modifies the extinction of starlight, particularly at very short wavelengths. Emission in the ultra-violet is dominated by hot, massive stars which have short lifetimes. The massive stars spend a significant fraction of their lifetime inside a molecular cloud, depending upon the time-scale adopted for the star to escape from the cloud, which is a parameter of the dust model (Granato et al. 2000). This hybrid scheme with diffuse and molecular cloud dust components mimics the more rigorous calculation of dust extinction carried out by the spectrophotometric code *GRASIL* (Silva et al. 1998).

3 THE COUNTS OF EROS

Here we compare the abundance and redshift distribution of EROs and K-selected samples predicted by the two models with observations. We begin by considering how well the models reproduce the number counts of K-selected galaxies (§3.1), before presenting predictions for the surface density of EROs (§3.2). Redshift distributions are discussed in §3.3.

3.1 Total K-band number counts

The local K-band luminosity function is one of the datasets used to fix the values of the parameters which define each semi-analytical model. A comparison of the model predictions to these data is given in Baugh et al. (2005) and Bower et al. (2006). Bower et al. also show how the Baugh et al. and Bower et al. models compare against observational estimates of the rest-frame K-band luminosity function to $z=1.5$. In the Bower et al. model, there is remarkably little evolution at the bright end with redshift, in very good agreement with the observations. The Baugh et al. model does predict a modest but significant degree of evolution at the bright end.

Before considering the surface density of EROs, it is instructive to first look at the overall K-band number counts, which are sensitive to the evolution of the *observer* frame K-band luminosity function. The motivation for this is the following. A deficiency in the predicted number counts of EROs could be explained in part by the failure of a model to match the total galaxy counts. Fig. 1 shows¹ the differential

¹ The observed K-band counts are from the following sources, with symbols indicated in the Fig. 1 legend: Väisänen et al. (2000); Djorgovski et al. (1995); McCracken et al. (2000); Mobasher et al. (1986); Gardner et al. (1993, 1996); Glazebrook et al. (1995b); McLeod et al. (1995); Soifer et al. (1994); Huang et al. (1997, 2001); Moustakas et al.

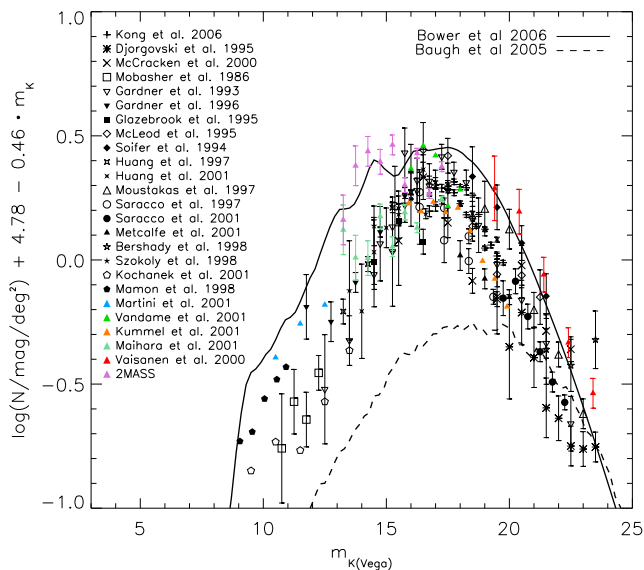


Figure 1. The differential K-band number counts, plotted after dividing by a power law (as given in the label on the y-axis) which is the one that best fits the observed counts. The solid line shows the counts predicted by the Bower et al. model and the dashed line shows the Baugh et al. model. The compilation of observed counts was kindly supplied by Nigel Metcalfe and can be downloaded from <http://star-www.dur.ac.uk/~nm/pubhtml/counts/kdata.txt>.

K-band number counts, after dividing by a power law fit to the observed counts to expand the useful dynamic range on the y-axis. What is plotted is effectively the deviation of the counts from the power law that best fits the compiled observational data. There is a considerable spread in the observed counts at bright magnitudes ($K < 15$), which could be a sign that surveys in particular directions are affected by a local hole in the galaxy distribution (e.g. Frith et al. 2006). The Bower et al. model is higher than many of the observed counts at these magnitudes, but does agree well with some of the datasets. The Baugh et al. model on the other hand underpredicts the bright counts by a factor of three. This discrepancy can be traced to a mismatch between the predicted and observed shape of the K-band luminosity function around L_* . The observed number counts are most sensitive to the form of the luminosity function close to L_* , whereas when assessing a plot of a luminosity function, the eye is naturally drawn to the faint and bright ends. The scatter between the various observational estimates of the counts is still almost a factor of two at faint magnitudes. At $K \sim 19$, the Baugh et al. counts are a factor of four lower than the prediction of the Bower et al. model. The Baugh et al. and Bower et al. model predictions bracket the observational data at $K \sim 19$ and converge at $K \sim 23$.

(1997); Saracco et al. (1997, 2001); Metcalfe et al. (2001); Bershady et al. (1998); Szokoly et al. (1998); Kochanek et al. (2001); Mamon (1998); Martini (2001); Vandame et al. (2001); Kümmel & Wagner (2001); Maihara et al. (2001); Kong et al. (2006)

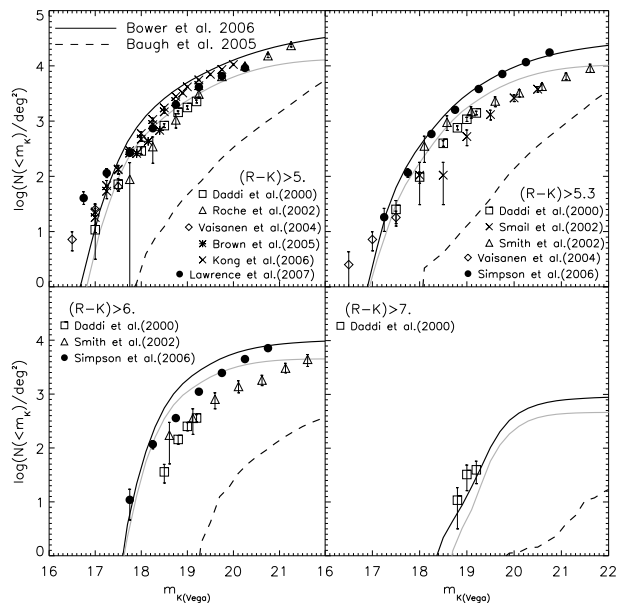


Figure 2. The cumulative K-band number counts for EROs selected by their $(R - K)$ colour: $(R - K) > 5$ – top left panel, $(R - K) > 5.3$ – top right panel, $(R - K) > 6$ – bottom left panel and $(R - K) > 7$ in the bottom right panel. The solid black lines corresponds to the predictions from Bower et al. and the dashed ones to the Baugh et al. model. The grey lines show the number counts of EROs in the Bower et al. model that are also central galaxies. The source of the observational data is given in the legend of each graph and the points can be found at: <http://segre.ieec.uab.es/violeta/rawEROSdata.txt>. The errors shown are Poisson.

3.2 The abundance of EROs

As we discussed in the Introduction, reproducing the abundance of EROs has previously eluded many hierarchical models, but is a necessary requirement for any model which aims to explain the nature of these objects. In Fig. 2 we compare the observed counts² with the predicted counts for samples of EROs defined by different colour cuts, $(R - K) > 5, 5.3, 6$ and 7 . The dispersion between observational estimates is due in part to the use of different filters, the application of different apertures to determine colours and sample variance due to the small fields used (Simpson et al. 2006). The predictions of the Bower et al. model reproduce the observed abundance of EROs impressively well, for all the colour cuts shown, which is remarkable as none of the model parameters have been tuned to achieve this level of agreement. The observational data for EROs defined by $(R - K) > 5$ show the least dispersion. These results are matched well by the Bower et al. model, except around $K = 18$ where the model slightly overpredicts the number counts by a factor of ~ 2 . Bower et al. overestimates the number counts of EROs with $(R - K) > 6$, particularly

² The observed ERO counts are from the following sources, with symbols indicated in Fig. 2 legends: Daddi et al. (2000); Roche et al. (2002); Smith et al. (2002); Smail et al. (2002); Väisänen & Johansson (2004); Brown et al. (2005); Simpson et al. (2006); Kong et al. (2006); Lawrence et al. (2007)

around $K = 19$ where the discrepancy is close to a factor of five.

The excess of EROs in the Bower et al. model could result from the star formation in massive galaxies being quenched too efficiently at high redshift by the AGN heating of the hot halo, which cuts off the supply of cold gas and hence leads to old stellar populations. An alternative explanation could lie in the treatment of satellite galaxies in the model. Typically in semi-analytical models, when a halo merges with another halo, the hot gas is assumed to be stripped completely from the smaller halo. The largest galaxy in the newly formed halo is called the central galaxy, and any gas which subsequently cools is directed onto this galaxy. Star formation in the satellite ceases when its reservoir of cold gas has been exhausted; this is sometimes referred to as “strangulation”. Motivated by the results of gas dynamics simulations of the efficiency of hot gas stripping by ram pressure from McCarthy et al. (2008), Font et al. (2008) presented a revised version of **GALFORM** in which satellites retain some fraction of their hot gas haloes, depending on their orbits. Font et al. found that this new model changes the fraction of satellites with red colours and gives a better match to the colour distribution of satellites in galaxy groups as determined from the Sloan survey by Weinmann et al. (2006). However, this extension of the gas cooling model is unlikely to have a significant impact on the predicted counts of EROs, since the galaxies whose colours are affected are primarily fainter than L_* . We show the contribution of central galaxies to the counts of EROs in Fig. 2. At faint magnitudes, satellites account for a substantial fraction of the ERO population, and the predictions of the Bower et al. model are in better agreement with the observed counts if satellites are excluded altogether. The Font et al. paper was in the final stages of being refereed when our paper was being prepared for submission; the number counts of EROs in the Font et al. model will be discussed in the other papers in this series.

The agreement is less impressive for the Baugh et al. model. Fig. 2 shows that this model typically underestimates the number counts of EROs by more than an order of magnitude. Appealing to scatter resulting from the small size of the fields surveyed to measure the ERO counts is overly optimistic. The errors shown in Fig. 2 are Poisson counting errors. EROs are believed to be strongly clustered (see Paper II) and so the Poisson error is a lower limit on the error, to which sampling variance in the spatial distribution of EROs should be added. However, it has been argued that this is unlikely to account for more than a factor of two scatter in number density (Somerville et al. 2004). Another possibility to improve the Baugh et al. predictions would be to force the model to agree with the overall K -band counts. In the previous section, we pointed out that at $K \sim 19$ the Baugh et al. model underpredicts the total counts by a factor of ~ 4 . One could imagine applying an equal correction to the predicted luminosities in all bands (to preserve galaxy colours), in order to force the Baugh et al. K -band counts to agree with the observations. Upon doing so there would still be a factor of 2.5 to 3 discrepancy with the observed ERO counts.

Some fraction of EROs are likely to be heavily dust extinguished, a point we return to in Section 4. It is therefore important to make a realistic calculation of the degree

to which galaxy colours are extinguished in order to be able to make robust predictions for the counts of EROs. As we shall see in the next subsection, the typical redshift of EROs with $(R - K) > 5$ is $z \approx 1$. The R-band samples the rest frame near ultra-violet ($\sim 3300\text{\AA}$) for a galaxy at this redshift. In our standard calculations we use a refinement of the dust extinction model introduced by Cole et al. (2000), as described in Section 2, in which the dust is assumed to be in two components, diffuse dust and molecular clouds. We have experimented with changing the fraction of dust contained in molecular clouds (the default choice is 25%) and do not find a significant difference in the predicted counts of EROs in the Baugh et al. model. We also repeated the calculation using the spectro-photometric code **GRASIL** (Granato et al. 2000; Lacey et al. 2008). Again, we find a similar amount of extinction to that obtained with the less expensive calculation carried out with **GALFORM** alone.

We shall see in the next section that the Baugh et al. model predicts very few dusty starburst EROs. This can also be connected to the lack of a break in the predicted shape of the ERO counts in Baugh et al.. The observations of both Kong et al. (2006) and Smith et al. (2002) show evidence for the presence of a break in the slope of number counts at $K \in [18, 19]$ for EROs with $(R - K) > 5$ and $K \in [19, 20]$ for EROs with $(R - K) > 5.3, 6$. This has led to speculation that there may be a change in the nature of EROs around this magnitude, with a transition from the dominance of old galaxies at low redshifts and to dusty starbursts at high redshift. No such feature is apparent in the Baugh et al. model, except for EROs with $(R - K) > 6$. To investigate if the lack of a break (and the overall deficit of ERO counts) is due to the choice of burst timescale adopted in Baugh et al., we reran the model with a burst time scale set to twice the bulge dynamical time, with a minimum allowed value of 1 Myr. The original parameter values adopted in Baugh et al. were 50 times the dynamical time with a minimum timescale of 200 Myr. Changing to a shorter burst duration had little impact on the predicted number of EROs.

The disagreement between the Baugh et al. model and observations suggests that the superwind feedback used in this model could be too efficient for bright galaxies at $z > 1$, delaying their formation, and that bursts of star formation maybe should also be allowed to be triggered by other events besides mergers (such as the dynamical instabilities of disks), in order to try to account for the larger observed number of red, dusty star-forming galaxies.

3.3 The redshift distribution of EROs

The colour criteria that classify a galaxy as an ERO are designed to select objects at $z \geq 1$ based on combining simple star formation histories with stellar population synthesis models (e.g. Thompson et al. 1999). However, the redshift selection can be different when dealing with hierarchical galaxy formation models, due to the rich variety of star formation histories that can be generated (see for example Baugh 2006). In this section we present the redshift distributions of EROs predicted by the Bower et al. and Baugh et al. models.

We start by testing the model predictions against observational data for K -selected galaxies, since EROs are a subsample of these. The predicted differential redshift dis-

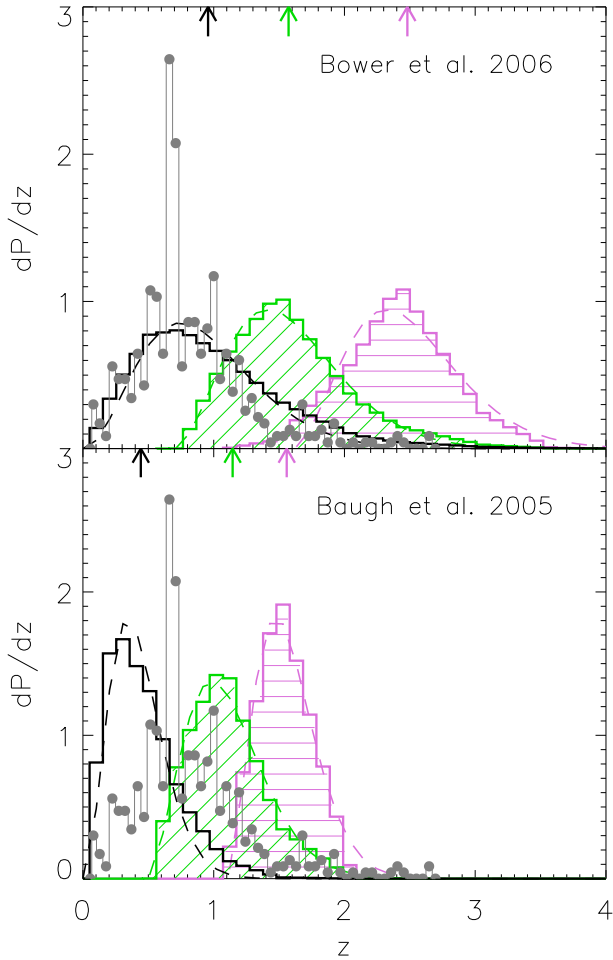


Figure 3. The redshift distribution of EROs with $K \leq 20$, defined by $(R - K)$ colour redder than 5 (histogram filled with sloping parallel lines) and 7 (histogram filled with parallel lines). The black histogram represents the redshift distribution for all galaxies with $K \leq 20$. Histograms are normalized to give unit area under each distribution. The arrows on the upper x-axis show the median of the distribution plotted with the same colour. Observational data from Cimatti et al. (2002b) for galaxies with $K \leq 20$ are shown as grey connected filled circles. The upper panel shows the predictions from Bower et al. and the lower one from the Baugh et al. model. The dashed curves show parametric fits to the model redshift distributions (see Eq. 1 and Table 1).

tributions of galaxies brighter than $K = 20$ are shown in Fig. 3, and are compared with the observational data from the K20 survey (Cimatti et al. 2002b). This survey covers an area of 52 arcmin^2 and contains 480 galaxies with $K \leq 20$. The spectroscopic completeness is 87%; most of the incompleteness is for galaxies at $z > 1$, for which it was particularly hard to extract redshifts, unless strong $H\alpha$ was present in emission. Where a spectroscopic redshift was not available, a photometric redshift was estimated using multi-band photometry. Observations by Cirasuolo et al. (2007) find a similar redshift distribution to that of the K20 survey, using a larger sample of galaxies, ~ 2200 in 0.6 deg^2 , but with only 545 spectroscopic detections and so a much heavier reliance on photometric redshifts. The spike in the K20 redshift distribution at $z \sim 0.7$ is due to the pres-

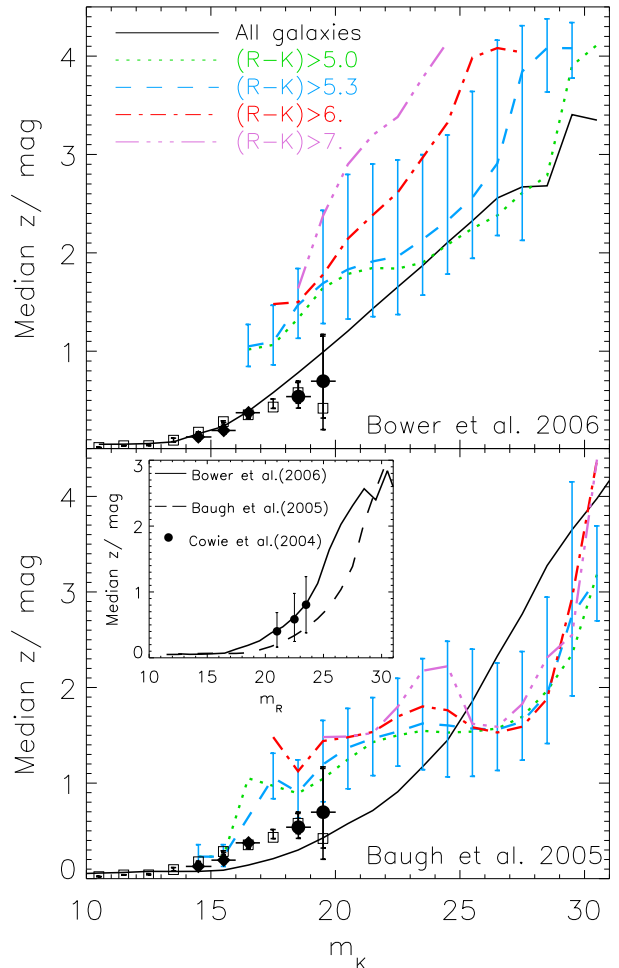


Figure 4. The median redshift as a function of K band magnitude for all galaxies (solid line) and for EROs with $(R - K)$ colour redder than 5 (dotted line), 5.3 (dashed line), 6 (dash-dotted line) and 7 (dash-triple dotted line). For clarity, quartiles are only shown for EROs with $(R - K) > 5.3$. The upper panel shows predictions from Bower et al. and the lower one from Baugh et al.. For comparison we plot the median redshift for all galaxies per magnitude bin in the K-band observed by Songaila et al. (1990) (squares), Glazebrook et al. (1995a) (diamonds) and Cowie et al. (1996) (circles). The inset shows the median redshift per magnitude bin in the R-band for all galaxies predicted by Bower et al. (solid line) and Baugh et al. (dashed line), and the observational data from Cowie et al. (2004) (filled circles).

ence of two clusters. Ignoring this spike, it can be seen that Bower et al. makes an accurate prediction of the redshift distribution of K-selected galaxies out to $z \sim 1.3$. At higher redshifts, the Bower et al. model overpredicts the number of objects. This is reinforced by the fact that the median redshift predicted by Bower et al. model, $z_{\text{med}} = 0.96$, is comparable to but slightly higher than that observed by Cimatti et al. (2002b), $z_{\text{med}} = 0.805$ (excluding the two clusters; $z_{\text{med}} = 0.665$ otherwise). Such good agreement is in contrast with the Baugh et al. model which predicts a narrower redshift distribution around a lower redshift value, $z_{\text{med}} = 0.42$. Fig. 3 shows that the observation of significant numbers of galaxies with $z > 1$ favours the Bower et al.

Table 1. Best fits to the redshift distributions predicted by the Bower et al. and Baugh et al. models, as described in §3.3. The first column gives the K -band magnitude limit and the second gives the colour selection applied. Columns 3, 4, 5, 6 give the best fitting parameters and the value of the summed squared residuals under χ^2 for the Bower et al. model; columns 7 to 10 give the equivalent quantities for the Baugh et al. model.

$K \leq$	$(R - K) >$	Bower et al.				Baugh et al.			
		A	z_c	α	χ^2	A	z_c	α	χ^2
20.	none	5.825	0.616	-	0.100	58.111	0.284	-	0.359
	5.0	6.681	0.604	0.683	0.032	19.846	0.424	0.474	0.067
	5.3	11.222	0.501	0.930	0.074	10.996	0.519	0.493	0.059
	6.0	10.352	0.518	0.968	0.085	29.846	0.367	0.996	0.297
	7.0	6.608	0.608	1.588	0.199	44.581	0.325	1.083	0.131
18.	5.3	55.775	0.297	0.723	0.062	73.358	0.265	0.737	0.333
22.	5.3	6.014	0.616	0.890	0.086	14.774	0.464	0.859	0.209

model; in the Baugh et al. model it is much less likely that one would find galaxies at such redshifts.

For further comparison, we plot in Fig. 4 the observed median redshift distributions for both the K (Songaila et al. 1990; Glazebrook et al. 1995a; Cowie et al. 1996) and R bands (Cowie et al. 2004) and compare with the model predictions. The Bower et al. model is consistent with the observations in both bands. The Baugh et al. model matches the data better in the R -band than it does in the K -band. The Baugh et al. model underestimates the median redshift for K -selected samples faintwards of $K \sim 16$.

Both Fig. 3 and Fig. 4 show predictions for samples of EROs defined by different colour cuts. The most common way of selecting EROs is by imposing $(R - K) > 5.3$. Nevertheless different definitions have been used in observational studies which results in different properties (see McCarthy 2004). The Bower et al. (Baugh et al.) model predicts the median redshifts to be $z_{\text{med}} = 1.57(1.12), 1.77(1.52)$ and $2.48(1.53)$ for galaxies with $K \leq 20$ redder than $(R - K) = 5, 6$ and 7 , respectively. As expected from stellar population synthesis models, the median redshift of EROs is $z_{\text{med}} \sim 1$ or higher, independent of the colour cut and model; this also explains why there are few EROs at very bright K -band magnitudes. Cimatti et al. (2003) measured a median redshift of $z_{\text{med}} \sim 1.27$ for a sample of EROs with $(R - K) > 5$ and $K \leq 20$, which was only 62% complete spectroscopically. Other surveys using a mixture of spectroscopic and photometric redshift determinations find similar results: for EROs with $(R - K) > 5$, Moustakas et al. (2004), with a limiting magnitude of $K = 20$, measured a median redshift of $z_{\text{med}} \sim 1.20$, whereas Brown et al. (2005), with a brighter cut of $K < 18.4$, found $z_{\text{med}} \sim 1.18$. As expected from the above discussion, these values are somewhat higher than the predictions of the Baugh et al. model and lower than the Bower et al. predictions.

Within the UKIDSS survey data, Simpson et al. (2006) found a clear tendency for redder EROs to be at higher redshifts. In Fig. 3 the same tendency is predicted by the Bower et al. model. This trend is also present in the Baugh et al. model but is less pronounced than in the Bower et al. model. According to Fig. 3 and Fig. 4, the Baugh et al. model predicts few galaxies beyond $z \sim 1.5$ in simple K -selected samples. However, on applying a colour cut, the median redshift increases sharply: for galaxies with $K < 20$ and $(R - K) > 6$, the median redshift is $z \sim 1.5$.

Thus, even in the Baugh et al. model, which on the whole tends to predict shallower redshift distributions than are observed, redder ERO samples probe higher redshifts ($z > 1$).

The shape of the redshift distribution can be parameterized using the simple parametric form introduced by Efstathiou et al. (1991):

$$\frac{dN}{dz} = Az'^2 \exp \left[- \left(\frac{z'}{z_c} \right)^\beta \right], \quad \text{for } z' > 0, \quad (1)$$

where A is a normalization parameter in units such that dN/dz gives the number of galaxies per square degree per unit redshift, β controls the shape of the distribution and z_c is related to the median redshift of the distribution as a function of β . EROs are not found at low redshifts, therefore we introduce an offset to the distribution, $z' = z - \alpha$. When fitting the redshift distribution of K -selected galaxies we do not need this offset, since these galaxies are expected to populate the low redshift range.

The best fit parameters for the redshift distributions predicted by the Bower et al. and Baugh et al. models are listed in Table 1. Baugh & Efstathiou (1993) found that $\beta = 3/2$ gave a good description of the shape of the redshift distribution for B -selected samples. We find that the same value of β also gives a good match to the shape of the samples considered here, so we hold $\beta = 3/2$ fixed. As can be seen in both Table 1 and Fig. 3, the empirical model described by Eq. 1, accurately reproduces the model predictions. The median redshift z_{med} is related to z_c for $\beta = 3/2$ as follows (Baugh & Efstathiou 1993):

$$z_{\text{med}} = 1.412z_c + \alpha. \quad (2)$$

Extracting the median redshift from Table 1, we again find the tendency for redder galaxies to be at higher redshifts.

The last two rows in Table 1 list the best fit parameters for the redshift distribution of EROs redder than $(R - K) = 5.3$ with magnitudes limits different from $K = 20$. The median redshift is readily obtained directly from the fit; for the Bower et al. (Baugh et al.) model the median derived in this way is $z_{\text{med}} = 1.13(1.11), 1.65(1.23)$ and $1.85(1.53)$ for EROs with $(R - K) > 5.3$ and brighter than $K = 18, 20$ and 22 , respectively. Thus from this it is clear that with progressively fainter limits we observe more distant galaxies.

By its definition, α gives an estimation of the redshift at which EROs start to appear. It can be seen from Table 1, that for $K \leq 20$, EROs defined with redder cuts

start to appear at higher redshifts. However, this tendency is less clear for fainter magnitude limits. This could be due to the fact that samples defined by $K > 20$ already probe higher redshifts, so there is less variation on changing the colour cut. Bergström & Wiklind (2004) studied in detail at what redshift galaxies can be classified as EROs, based on the spectral evolution synthesis model PEGASE2. They found out that galaxies with star formation histories matching those inferred for ellipticals will show colours as red as $(R - K) = 5$ for redshifts $z \geq 0.6$, depending on the metallicity assumed. These authors also found that starburst galaxies could be detected as EROs, i.e. with $(R - K) > 5$, at redshifts around $z = 5$ for an extinction of $E(B - V) \leq 1$, or at lower redshifts for stronger extinctions, on assuming a Calzetti et al. (2000) extinction law. The redshift that Bergström & Wiklind (2004) proposed for the emergence of passively evolving EROs is similar to the prediction for all EROs by the Bower et al. model, though is a bit higher than suggested by the Baugh et al. model.

Since the work of Bergström & Wiklind (2004) is based on combining stellar population synthesis models with simple star formation histories, it is important to compare the semi-analytical model predictions directly with observations. Fig. 5 shows the predictions of the Bower et al. and Baugh et al. models for the redshift distribution of EROs with $(R - K) > 5$ classified according to either their star formation activity or morphological type. In this plot, the distinction between the *old* and *starburst* populations depends on whether or not the galaxy is undergoing or recently experienced an episode of star formation triggered by a galaxy merger or by a dynamically unstable disk. A model ERO is classified as a *starburst* if it is undergoing such a starburst, or if one happened within the past 1 Gyr. Note that we investigate an alternative definition of activity in Section 4.2 based on the specific star formation rate, and find that, with a suitable choice of specific star formation rate, we obtain similar numbers of “active” and “passive” galaxies as we do when the activity is considered to have been triggered by some event, as is the case in this section. For morphological classification, we use the bulge-to-total luminosity ratio in the observer-frame K-band, B/T . Further details of the definitions of the various classes of galaxies will be given in section 4.

It can be seen in Fig. 5 that both the Bower et al. and Baugh et al. models predict that quiescent galaxies appear as EROs at redshifts $z \geq 0.7$, in agreement with the expectations of Bergström & Wiklind (2004). Nevertheless, both models show starburst galaxies with ERO colours at redshifts lower than $z = 5$, though none of these galaxies are predicted by the Bower et al. model to have $E(B - V) > 1$ (see next section), as was assumed (albeit for a different extinction model) by Bergström & Wiklind (2004). Fig. 5 includes Cimatti et al. (2002a) observational data. Cimatti et al. (2002a) classify galaxies as old if they have a prominent 4000\AA break and no emission lines, and as starbursts if they do show emission lines. The Baugh et al. redshift distribution of old EROs matches the observed one. However, it is notable that this model predicts no dusty starbursts with the colours of EROs. In the Baugh et al. model, there are sufficient dusty starbursts to account for the sources detected by SCUBA, mostly at somewhat higher redshifts than relevant here for EROs. The Bower et al.

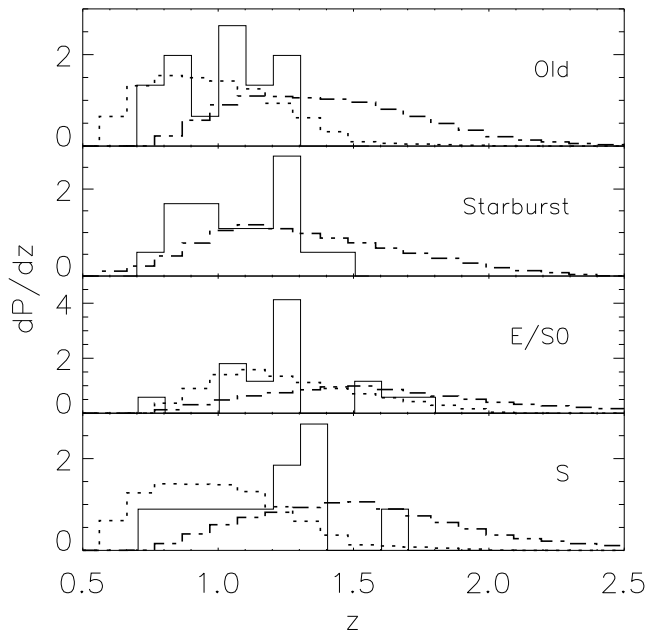


Figure 5. The redshift distribution of EROs with $(R - K) > 5.0$, predicted by Bower et al. (dash-dotted line) and Baugh et al. (dotted line), compared with the observational data from Cimatti et al. (2002a) and Cimatti et al. (2003) (solid line). The magnitude limits for the EROs are $K = 19.2$ for the two upper panels and 20 for the two lower panels respectively. From top to bottom the redshift distributions are plotted for quiescent or old galaxies, galaxies that are experiencing a burst of star formation (note that there is no dotted line in this panel, as the Baugh et al. model does not predict starburst EROs), spheroidal galaxies and spiral ones (see text for further details on the classification). Histograms are normalized to give unit area under each distribution.

model overpredicts the high redshift tail of the starburst distribution, however the incompleteness of observations at these redshifts could account for this mismatch.

Fig. 5 also shows the predicted redshift distribution for different morphological types compared to the observational data from Cimatti et al. (2003). Their classification is based upon visual inspection of images in the observer-frame B, V, i and z bands. It can be seen that Baugh et al. model predicts a redshift distribution for spheroidal EROs which is quite close to the observed one, while the Bower et al. model overpredicts, again, the high redshift tail. In the case of disk-dominated galaxies the mismatch for both models increases, with the Baugh et al. model predicting too few high redshift galaxies and Bower et al. too many.

In summary, the Baugh et al. model tends to predict shallower redshift distributions than the observations for all EROs, while Bower et al. is in better agreement with the data. However, the Baugh et al. model better matches the observed redshift distribution of both old and spheroidal EROs. It seems that the Baugh et al. model underpredicts the number of disk dominated galaxies, particularly at redshifts higher than $z \sim 1$. For different types of EROs the Bower et al. model consistently overpredicts the number of galaxies in the high redshift tail. This is perhaps an indication that the star formation is quenched too early in massive galaxies in this model. However, it should be borne in mind

that the observations we are comparing to are affected by cosmic variance and by incompleteness at high redshift.

4 THE NATURE OF EROS

In the previous section we presented the predictions of the Baugh et al. and Bower et al. models for the number counts and redshift distribution of EROs. The Bower et al. model gave a better match to the observations in both instances, and for this reason we restrict our investigation of the predicted properties of EROs to this model. In addition to underpredicting the abundance of EROs by a large factor, the Baugh et al. model does not predict any dusty starburst EROs. Therefore the properties of EROs in this model are of limited interest, since we do not know how they compare with the properties of the “missing” EROs, which could be substantially different.

In this section, we investigate whether or not EROs form one or more distinct populations of galaxies, or if there is a continuous range of intrinsic properties, marking a gradual transformation of active, massive galaxies to passive objects, as suggested by Conselice et al. (2008). Observationally, EROs exhibit a mixture of morphologies and spectral properties (e.g. Smail et al. 2002). At the epoch when EROs are detected, $z \geq 1$, the star formation rate per unit volume is much higher than it is today and the range of galaxies which are undergoing significant additions to their mass is much broader than is inferred locally (e.g. Abraham et al. 2007). Thus, the connection between a galaxy’s morphology and its spectral energy distribution cannot be assumed to be the same as it is for nearby galaxies. In fact, Smail et al. (2002) pointed out that the visual classification of EROs did not match their spectral energy distributions (SED). Consequently, in this section we study the nature of EROs by analyzing separately their morphology and their level of star formation activity, the primary agent which shapes a galaxy’s SED.

4.1 The morphology of EROs

Semi-analytical models track the amount of light in the spheroid and disk components of model galaxies (e.g. Baugh et al. 1996). A simple proxy for morphological classification is therefore the bulge to total luminosity ratio, B/T . Here, we use this ratio measured in the observer frame K-band to apply a morphological classification to the model galaxies. Different observational studies have used images in different bands to make morphological classifications, so our choice is necessarily a compromise and we are more interested in the trends with B/T ratio than with absolute values. There is a large scatter between the bulge to total luminosity ratio and other indicators of morphology such as the subjective Hubble T-type (Simien & de Vaucouleurs 1986). Despite this, we follow the results of Simien & de Vaucouleurs and adopt a boundary between early-type (bulge dominated) galaxies and late-type (disk dominated) galaxies at $B/T = 0.4$. Our results are insensitive to the precise choice of this value. We note that one potential flaw in this scheme is that irregular and interacting galaxies are not naturally accommodated into the B/T classification whereas, observationally, they become a more important population

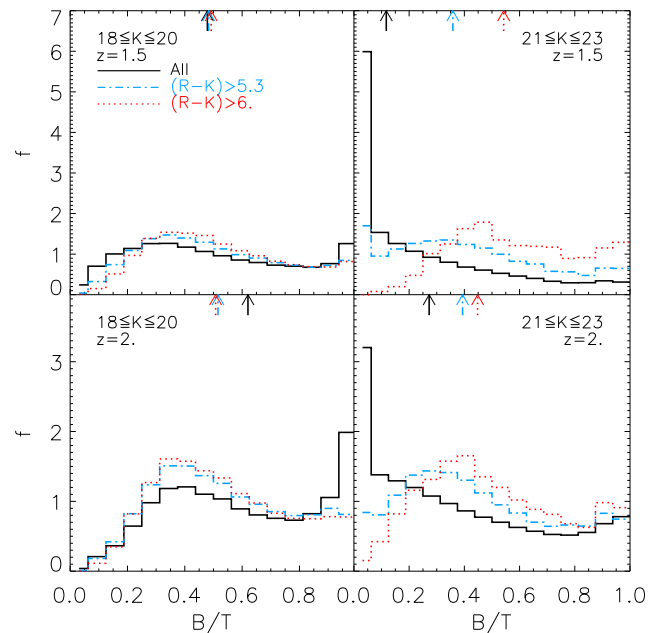


Figure 6. The predicted distribution of galaxy bulge to total luminosity ratio, in the observer frame K-band, in the Bower et al. model. The top row shows $z = 1.5$ and the bottom shows $z = 2$. The panels in the left-hand column correspond to an apparent magnitude range of $18 \leq K \leq 20$ and the right hand panels show $21 \leq K \leq 23$. K -selected galaxies distribution appear as a solid line. EROs distributions are represented by the dotted, $(R - K) > 5.3$, and dash-dotted histograms, $(R - K) > 6$. The arrows show the median bulge to total ratio for the histogram plotted with the same line style.

with increasing redshift, particularly around the typical redshift of ERO samples (e.g. Abraham et al. 2007). Ultimately, the broad brush nature of our morphological classification will limit how closely we can compare the model predictions to observational results.

Fig. 6 shows the predicted distribution of B/T in the Bower et al. model for $z = 1.5$ and $z = 2$ in two different apparent magnitude ranges. This plot shows that it is more likely to find K -selected galaxies with late-type B/T ratios in the fainter magnitude range than it is in the brighter magnitude bin. The same tendency is found for EROs, although it is weaker since the variation from one magnitude range to the other is smaller in this case than it is when simply K -selecting galaxies without a colour cut. Averaging over the redshift interval $1 \leq z \leq 2.4$, the predicted median B/T values for EROs with $(R - K) > 5.3$ (6) shifts from 0.42 (0.48) in the faint bin to 0.51 (0.53) in the bright one. The same tendency is observed by Moustakas et al. (2004), when considering as late-type EROs those not classified as early-type. Note, however, that these authors classified some interacting EROs as having early-type morphologies, which makes a direct comparison with our classification based on B/T values difficult.

Table 2 gives the predicted morphological mix of K -selected galaxies with $K \leq 23$, and EROs at redshifts $z = 1, 1.5, 2$ and 2.5 . A slight increase is apparent in the percentage of early-type K -selected galaxies with increasing redshift. This tendency is due to the fact that for a fixed apparent magnitude range, when we increase the redshift we

Table 2. The predicted morphological mix of galaxies in the Bower et al. model, expressed as a percentage of *early-type:late-type*, for galaxies with $K \leq 23$ at $z = 1, 1.5, 2$ and 2.5 , including EROs redder than $(R - K) = 5, 5.3, 6$ and 7 . We use the bulge to total luminosity in the observer frame K -band as a proxy for morphology, with $B/T = 0.4$ setting the boundary between early and late types.

$(R - K)$	z			
	1.0	1.5	2.0	2.5
All	28:72	35:65	45:55	53:47
5.0	63:37	55:45	59:41	65:35
5.3	59:41	59:41	60:40	66:34
6.0	-	67:33	66:34	69:31
7.0	-	-	67:33	70:30

are looking at intrinsically brighter galaxies, which, as we have seen in Fig. 6, are predominantly early-type. The same behaviour is seen for EROs. Independent of the colour cut used to define EROs, for $z > 1$ there is a slight increase with redshift in the percentage of EROs with early-type B/T ratios. It should be noted that due to the form of the redshift distribution of faint EROs with $(R - K) > 6$, the statistics at $z = 1.5$ are actually poorer than they are at $z = 2$. For $(R - K) > 6$ EROs, the increase in the proportion of galaxies that are early-types is clearer on comparing the change in B/T seen when moving from $z = 2$ ($B/T_{\text{median}} = 0.47$), to $z = 2.4$ ($B/T_{\text{median}} = 0.49$), where the statistics are much better. This trend is at odds with the observations of Conselice et al. (2008), which show a decrease in the fraction of compact EROs with increasing redshift, while the proportion of peculiar and interacting galaxies increases. As was mentioned before, it is not clear what range of B/T corresponds to irregular galaxies. Indeed, Conselice et al. (2008) observe that disks and distorted spheroids EROs have light concentrations that are consistent with both early and late-type classifications. These authors also found that although peculiar and early-type galaxies occupy quite different loci in the light concentration parameter space, disks and distorted spheroids occupy intermediate values. Thus, it is expected to be possible to separate peculiar from early-type galaxies using the B/T parameter alone only in a sample free of disks and distorted spheroids. Otherwise, one would expect to find a distribution of galaxies with B/T values varying smoothly across the full dynamical range, from 0 to 1. The lack of bimodality is borne out by the smooth distribution of the predicted values of B/T plotted in Fig. 6.

Both Table 2 and Fig. 6 suggest that early-type EROs are redder, although the dependence of the morphological mix on both magnitude range and redshift is stronger. As can be seen from Fig. 4, the Bower et al. model predicts that at a given redshift it is more likely for redder EROs to be brighter. This is consistent with previous predictions since brighter EROs are more likely to exhibit an early-type morphology. Observations show just the opposite: peculiar galaxies appear to be redder (Moriondo et al. 2000; Smail et al. 2002; Smith et al. 2002). Nevertheless, with the observations of Moustakas et al. (2004) it is clear that this result is very sensitive to the magnitude range adopted and the incorporation of peculiar galaxies into the late-type class.

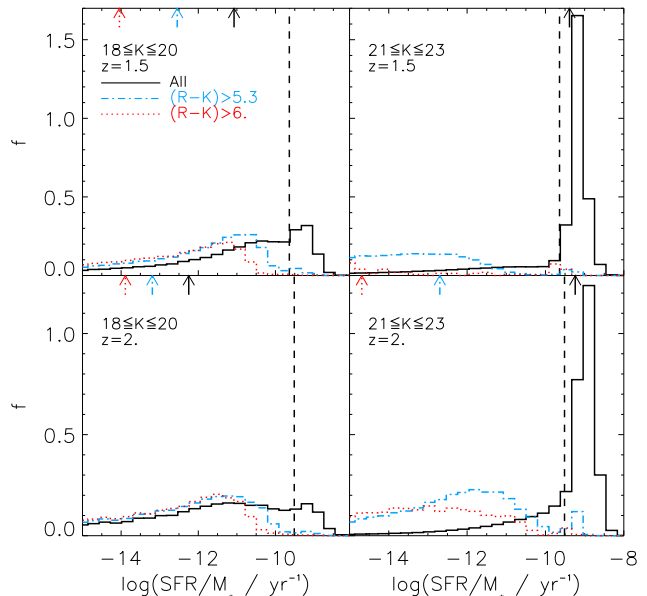


Figure 7. The distribution of the specific star formation rate predicted by the Bower et al. model, for different redshifts and K -band magnitude limits, as indicated in the legend within each panel. The arrows mark the median of the histogram drawn with the same line style. Median values for EROs in the upper right panel are out of the shown range. The vertical dashed lines indicate the inverse of the age of the universe at the labelled redshift.

4.2 Quiescent vs. Starburst EROs

We now consider the level of star formation activity in the model EROs. Galaxies with relatively high star formation rates can still possess the red colours associated with EROs if they are heavily extinguished. Alternatively, the red colour could arise from an old stellar population with little recent star formation.

We start by examining the specific star formation rate, SFR/M_* , that is, the star formation rate (SFR) per unit stellar mass. This ratio has dimensions of inverse time and is a measure of how rapidly the galaxy is adding to its stellar mass at the time of observation. If the specific star formation rate is comparable to the inverse of age of the universe at the epoch the galaxy is seen, then a substantial addition to the stellar mass is taking place. Fig. 7 shows the distribution of this parameter for samples of galaxies selected by K -magnitude and also by $(R - K)$ colour. The specific star formation rates of most galaxies are smaller than the inverse of the respective age of the universe at each redshift plotted, particularly so for the EROs. Only a small fraction of galaxies in the samples selected by K -magnitude alone are vigorously adding to their stellar mass. The distribution of the specific star formation is smooth, with no evidence for bimodality and little dependence on redshift or K -magnitude. The long tail of EROs with very low specific star formation rates suggests that for a large proportion of these objects the level of star formation activity is relatively unimportant and they are passively evolving, a point to which we return later on in this section.

Next we consider whether or not the star formation rate correlates with extinction for EROs. For a galaxy with a relatively high star formation rate to meet the colour criteria to

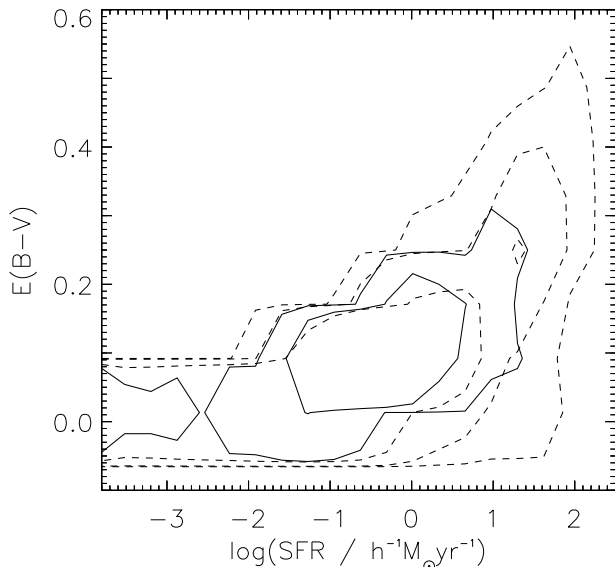


Figure 8. The dust extinction, as quantified through $E(B - V)$ versus star formation rate (SFR) predicted by Bower et al. at $z = 1$ (solid contours) and $z = 1.5$ (dashed contours) for EROs with $K \leq 20$, and $(R - K) > 5.3$.

be called an ERO, we would expect a correspondingly high level of extinction. In Fig. 8 we plot the extinction (see § 2 for a brief description of the extinction model), as quantified by $E(B - V) = (B - V)_{\text{with dust}} - (B - V)_{\text{no dust}}$, with the filters defined in the rest frame, against star formation rate. Each contour represents a change in the number density of galaxies by a factor of 10. There is a weak trend of extinction increasing with star formation rate, but only for rates above $\log(SFR/h^{-1}M_{\odot}\text{yr}^{-1}) > -0.5$. The model predicts that EROs have a wide range of extinctions, with colour excesses varying from 0 to ~ 0.6 . A little over $\sim 10\%$ of EROs have a colour excess $E(B - V) > 0.1$; these are also the most actively star forming galaxies.

The comparison between the values of $E(B - V)$ predicted by the model and empirical estimates in the literature is not straightforward. Typically, empirical estimates are made by assuming an extinction law and that the dust is in a screen in front of the stars and that no scattered light reaches the observer. As described in Section 2, in the model we assume that the dust and stars are mixed together and that some of the dust is in the form of molecular clouds (see Granato et al. 2000, for a discussion). In this case, the attenuation of starlight depends upon the randomly assigned inclination angle of the disk. We adopt a Milky Way extinction law; however, the attenuation *observed* in practice for a model galaxy is a function of the viewing angle and wavelength (see fig. 11 of Granato et al. 2000). For these reasons, it is of limited use to compare actual values of $E(B - V)$ unless the same assumptions have been made. We note in passing that Nagamine et al. (2005) were forced to fix an extreme colour excess of $E(B - V) = 0.4$ in a foreground screen extinction model with a Calzetti et al. extinction law in their gas dynamical simulations in order produce enough EROs. Here we have shown that with an *ab initio* calculation of the dust extinction, such an extreme assumption is not supported.

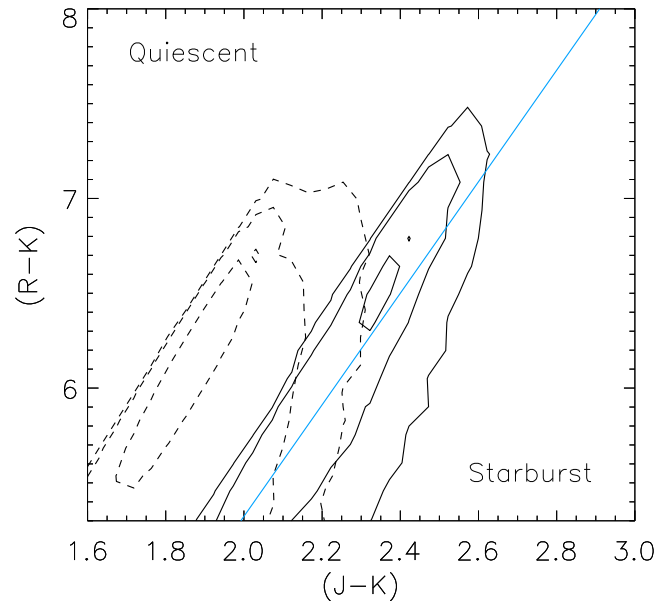


Figure 9. The Pozzetti & Mannucci (2000) colour-colour diagram for galaxies with $18 \leq K \leq 20$, at redshift $z = 2$ (solid contours) and $z = 1.5$ (dashed lines) as predicted by the Bower et al. model. The sloping solid line was proposed by Pozzetti & Mannucci to divide the colour-colour plane into regions occupied by quiescent galaxies (to the left of the line) and starbursts (to the right). Each contour in the plot represents a change by a factor of 10 in the number density of galaxies.

Despite the tendency for EROs that are actively star forming to also be dustier, we find little evidence for any distinct bimodality. There appears to be a continuous variation in extinction and star formation rate, with no obvious place to separate EROs into distinct populations that are either passive or active and dusty. Another way to look at this issue is in the $(R - K)$ vs $(J - K)$ colour-colour plane, as proposed by Pozzetti & Mannucci (2000). These authors suggested that EROs with $(R - K) > 5.3$ in the redshift range $1 \leq z \leq 2$ could be classified as either *quiescent* or *starburst* galaxies according to their location on the $(R - K)$ vs. $(J - K)$ colour diagram (see Fig. 9). This scheme has been shown to work observationally in $\sim 80\%$ of cases by comparing spectral templates to galaxies on either side of the dividing line in the colour-colour plane (e.g. Miyazaki et al. 2003). In the model, additional information is available to us about the star formation and merger history of each galaxy, such as the lookback time to the last burst of star formation triggered by a galaxy merger or by the collapse of an unstable disk. Hence, in addition to using the location of a galaxy in the colour-colour plane, we can also employ a classification based on the time of the most recent burst of star formation:

- *Quiescent*: Passively evolving galaxies, whose last burst of star formation occurred more than 1 Gyr ago.

- *Starburst*: This classification includes galaxies that are either experiencing a burst (which we will refer to as *bursty*) when they are observed or which have experienced a burst of star formation within the past 1 Gyr (which we shall call *post-burst*).

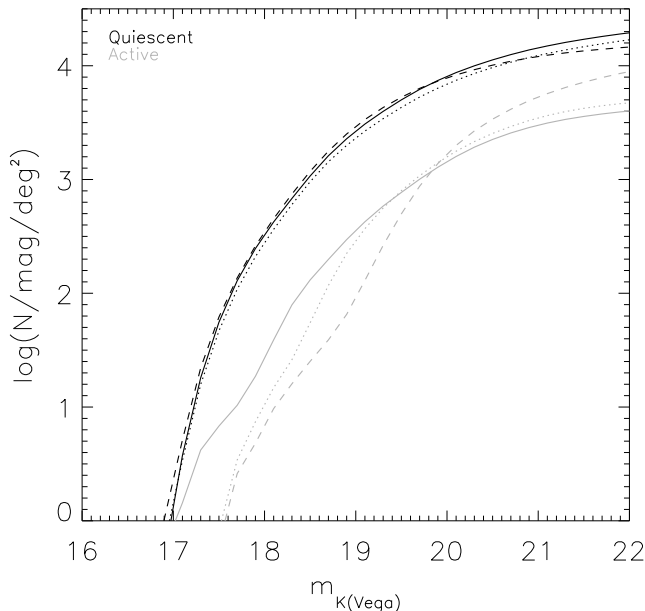


Figure 10. The number counts of EROs with $(R - K) > 5.3$, as predicted by the Bower et al. model, split into two populations. The black lines in each case show the counts for the “quiescent” part of the population. The different grey lines refer to “active” population defined according to: 1) the time since the last episode of star formation triggered by a galaxy merger or the collapse of an unstable disk (solid lines); this is our standard definition of a starburst galaxy; 2) whether the galaxy occupies the “starburst” locus in the Pozzetti & Mannucci color-colour diagram (dashed lines - see Fig. 9 diagram), or 3) the magnitude of the specific instantaneous star formation rate (dotted lines - see text for further details).

Post-burst EROs have been distinguished observationally from passively evolving galaxies by Doherty et al. (2005), who found that almost 40% of the EROs dominated by an old stellar population had spectral indications of the occurrence, within the last ~ 1 Gyr, of a secondary episode of star formation, in which a small percentage, $\sim 7\%$, of the total galactic mass was formed.

We compare in Fig. 10 the cumulative number counts of EROs predicted by the Bower et al. model, classified as *quiescent* or *starburst* using the two methods described above i.e. the location in the colour-colour plane, or the occurrence of the last burst of star formation. Fig. 10 shows that the counts of *quiescent* EROs as defined by their colour or the time since the last starburst, agree spectacularly well. This population dominates over the active or dusty starburst EROs. In the active case, the counts corresponding to the different definitions are not in such good agreement, so it is hard to conclude that the alternative definitions of active galaxies pick out similar objects. In one sense our definition of starburst is flawed in that quiescent galaxies could be experiencing similar star formation rates in their galactic disks, with the only distinction being that this star formation was not triggered by a galaxy merger or an unstable disk.

We have also investigated a third scheme to divide model EROs into active and passive populations, based on the magnitude of the specific star formation rate, i.e. the in-

Table 3. The predicted mix of *starburst:quiescent* galaxies (see text for definitions) in the Bower et al. model, for K-selected galaxy samples and for EROs with $18 \leq K \leq 20$ at $z = 1, 1.5, 2$. EROs are defined with different colour cuts, as indicated.

Classification Scheme	$(R - K)$	z		
		1.0	1.5	2.0
Burst occurrence	All	18:82	24:76	39:60
	5.0	1:99	12:88	24:76
	5.3	0:100	10:90	21:79
	6.0	-	5:95	12:88
Colour-Colour Pozzetti & Mannucci (2000)	All	34:64	20:80	43:57
	5.3	15:85	1:99	25:75
	6.0	-	0:100	14:86

stantaneous star formation rate divided by the stellar mass of the galaxy. The specific star formation rate quantifies the contribution of the current episode to the total stellar mass. A high specific star formation rate means that the current star formation will have a observable impact on the overall galaxy colour or on the visibility of line emission against the stellar continuum. With this definition, the classification into active and passive does not depend upon some triggering event, such as a galaxy merger or the dissolution of an unstable disk. This means that the active ERO population could be made up of “quiescent” disks or vigorous starbursts. In Fig. 10, we find similar results to those obtained in the two classification schemes discussed above if we place the division at a specific star formation rate of $SFR/M_* = 10^{-11} \text{yr}^{-1}$.

Table 3 summarizes the predicted percentages of *quiescent* and *starburst* galaxies for K-selected samples and for EROs, according to the classification methods outlined above. The magnitude range has been chosen to be close to that used in observations. Spectroscopic studies of EROs, with $(R - K) > 5$ or 5.3 and magnitude limits around $K \sim 20$ (e.g. Smail et al. 2002; Simpson et al. 2006), find roughly equal numbers of passively evolving and dusty star forming EROs. Similar ratios were found in observational studies (e.g. Mannucci 2002; Cimatti et al. 2003) that used the Pozzetti & Mannucci color-colour diagram to distinguish between *quiescent* and *starburst* EROs. Therefore, the predicted mix of *quiescent* and *starburst* EROs does not match the observations. The Bower et al. model underpredicts the number of dusty star forming EROs. This is likely to be due to the predicted scarcity, $\leq 1\%$, of *bursty* galaxies among EROs. This result can be connected with the number counts and redshift distribution of EROs, which suggest the need to review the star formation at $z > 1$ in the Bower et al. model. Either the star formation is quenched too soon due to a lack of cold gas or the burst timescale is too short.

Table 3 shows the tendency for the percentage of galaxies classified by the lookback time of the burst as *quiescent* to fall with increasing redshift. This matches the expectation for young galaxies to become the dominant population at high redshift. Nevertheless, this tendency is not as clear when the classification is made following the Pozzetti & Mannucci (2000) colour-colour method.

No clear dependency is found in the ratio between *quiescent* and *starburst* for K-selected galaxies with mag-

nitude range. The same can be said for EROs classified with the Pozzetti & Mannucci (2000) method. However, the percentage of *quiescent* EROs, defined by the occurrence of their last burst, increases by $\sim 12\%$ from a bright magnitude range, $18 \leq K \leq 20$, to a faint one, $21 \leq K \leq 23$. Cimatti et al. (2002a) observed the opposite tendency, though with a smaller variation (a $\sim 4\%$ change). Comparing observations from studies with different magnitude limits (Roche et al. 2002; Cimatti et al. 2002a, 2003; Miyazaki et al. 2003; Väisänen & Johansson 2004) no clear tendency is seen. Smith et al. (2002) proposed that the change in the slope of ERO number counts evident in Fig. 2 is due to a change in the nature of bright and faint EROs.

From Table 3 there is a clear tendency for the reddest EROs to be dominated by quiescent galaxies, independent of the classification method. The same tendency was found by Simpson et al. (2006), whose sample of EROs, was classified into old and starburst using the Pozzetti & Mannucci (2000) method.

Finally, following the scheme set out by Malbon et al. (2007), the models trace the growth of supermassive black holes, so in principle it is possible to identify if an ERO also has some sort of nuclear activity. The mass of the black hole may grow through mergers of pre-existing black holes, the accretion of cold gas during a starburst or the accretion of cooling flow gas in a quasi-static halo. The accretion of cold gas during mergers is usually associated with a QSO phase and the feeding of the black hole from the cooling flow with a “radio mode” of activity (Croton et al. 2006). The timescale for the “radio mode” activity is ill-defined in the model. Some fraction of the mass that would be involved in a cooling flow is diverted onto the black hole and the energy released stifles the cooling. This is assumed to operate over the lifetime of the halo.

In the case of QSO activity, the timescale for the accretion of cold gas onto the black hole is specified more transparently, but is poorly constrained. The choice of timescale has an impact on the luminosity of the QSO and so is chosen to reproduce the QSO luminosity function (Malbon et al. 2007). With the current choice of parameters for these timescales, none of the EROs modelled by Bower et al. show QSO activity. Observations suggest that the presence of AGNs among EROs is rare, and when present they are likely to be in a weak phase, rather than in a QSO state. Roche et al. (2002) detected 5 (16%) EROs with radio emission that was compatible with a weak AGN, and 1 (3%) were detected in X-ray, which suggested an AGN in a stronger phase. Smail et al. (2002) estimated that 6% of their radio detected EROs were AGNs.

5 OTHER PROPERTIES OF EROS

In this section we explore the model predictions for basic properties of EROs, such as luminosity, stellar mass, host halo mass, galaxy size and age. Given that the Bower et al. model gives the best match to the observed counts of EROs, we shall again only show predictions from this model in this section.

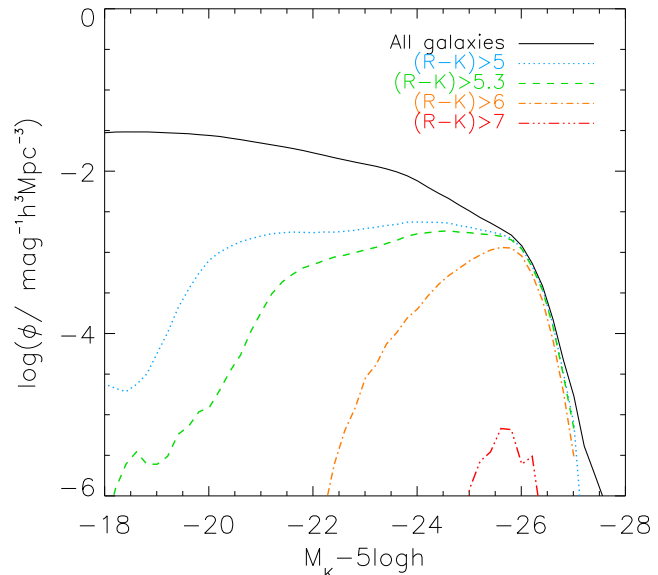


Figure 11. The K-band luminosity function in the observer’s frame predicted by the Bower et al. model at redshift $z = 1.5$, for all galaxies (solid line) and EROs redder than $(R - K) = 5$ (dotted line), 5.3 (dashed line), 6 (dash-dotted line), and 7 (dash-triple dotted line).

5.1 Luminosity

Fig. 11 shows the predicted K -band luminosity function at $z = 1.5$, for all galaxies and for different samples of EROs defined by $(R - K)$ colour. Bower et al. showed that the luminosity function of all galaxies in the K -band agrees well with the available observations up to $z \sim 1.5$. Fig. 11 shows that faintwards of L_* , only a fraction of galaxies have the colour required to be classified as an ERO. Furthermore this fraction falls dramatically with declining luminosity. The fraction of faint galaxies that are EROs also drops significantly as the $(R - K)$ colour threshold gets redder. Brightwards of L_* , however, essentially all galaxies are predicted to be EROs, until $(R - K) > 7$ is reached. This result matches the observations of Conselice et al. (2008), who found the reddest galaxies at $z \geq 1$ to be also the brightest in K-band.

5.2 Stellar mass

We first compare the predicted stellar masses in a K -selected sample with masses estimated from the K20 survey. The contours in Fig. 12 show the distribution of stellar mass for Bower et al. galaxies with $K < 20$ at $z=2$. Each contour represents a change in the number density of galaxies by a factor of 10. The dotted line shows a best fit to the stellar mass - K -band apparent magnitude relation. The dashed lines show the best fit to the mass estimated for galaxies in the same magnitude range around $z \sim 2$ in the K20 survey (Daddi et al. 2004). The two estimates correspond to the best fits when using the full photometry (lower line) or just one colour ($(R - K)$, termed the maximal mass estimate). Note that these curves have been shifted to account for the different stellar initial mass function (IMF) adopted by Fontana et al. (2004). Bower et al. adopt a Kennicutt (1983) IMF, whereas Fontana et al. use a Salpeter (1955)

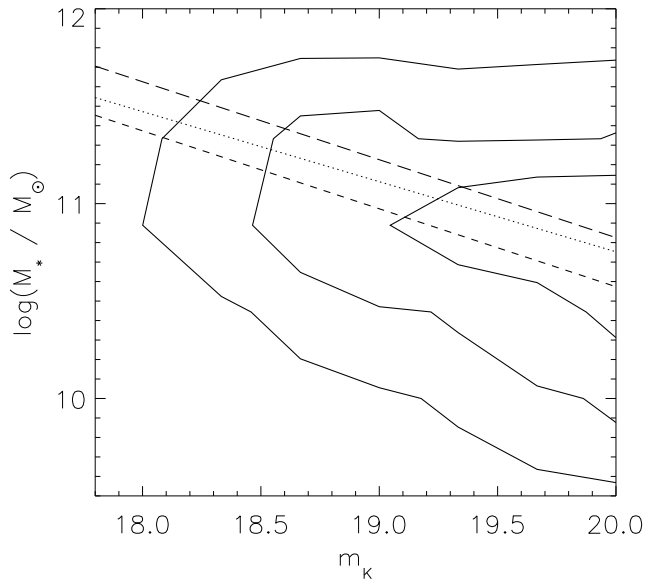


Figure 12. The number density of Bower et al. model galaxies with $K < 20$ at $z = 2$ in the stellar mass - K -band apparent magnitude plane (no colour selection is applied here). The dotted line shows the best fit stellar mass for the model. The two dashed lines show different estimates of the stellar mass of K20 survey galaxies made by Fontana et al. (2004), after applying an approximate correction to account for differences in the stellar initial mass function adopted in the two calculations.

IMF. The difference in mass to light ratio depends on star formation history and metallicity. Fontana et al. give some examples of how the mass to light ratios differ for these two choices of IMF. For a stellar population with age < 1 Gyr, they state that the mass to light ratio is a factor ~ 1.4 higher when using a Salpeter IMF compared with Kennicutt; the difference becomes a factor 2.2 for older populations. We have applied an indicative correction, dividing the masses inferred with a Salpeter IMF by a factor 1.7. The stellar masses estimated by Fontana et al. for K20 galaxies are in very good agreement with the model predictions.

We now compare the stellar masses of samples defined by a K -band selection and a $(R - K)$ colour threshold. Fig. 13 shows the stellar mass distribution of galaxies at redshifts $z = 1.5$ and 2, in two magnitude bins: $18 \leq K \leq 20$, which probes the region around L_* in the luminosity function and $21 \leq K \leq 23$, which is sensitive to the faint end of the luminosity function at these redshifts. Fig. 13 clearly shows the tendency for redder galaxies to be more massive, independent of the redshift or magnitude range. This distinction in the mass of EROs is more pronounced for the fainter magnitude range, due to the smaller fraction of EROs.

At $z = 1.5$, the Bower et al. model predicts that galaxies with $21 \leq K \leq 23$ have a median stellar mass of $\sim 1.8 \times 10^9 h^{-1} M_\odot$, while the median mass of the subset of these galaxies which are also redder than $(R - K) = 5.3$ (6) is appreciably higher, $\sim 3.6 \times 10^9 h^{-1} M_\odot$ ($\sim 6.8 \times 10^9 h^{-1} M_\odot$). Therefore, EROs are predicted to be the most massive galaxies present at the time. Bower et al. predicts that EROs are indeed the most massive galaxies in the redshift range $1 \leq z \leq 2$. In particular, at $z = 1.5$, EROs with $(R - K) > 5.3$

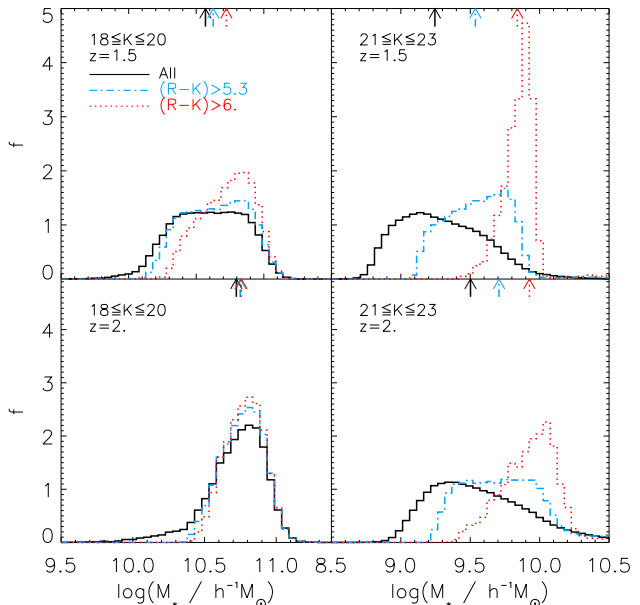


Figure 13. The distribution of stellar mass in the Bower et al. model for galaxies at $z = 1.5$ (upper panels) and $z = 2$ (lower panels) in the magnitude ranges $18 \leq K \leq 20$ (left panels) and $21 \leq K \leq 23$ (right panels). In each panel, the distribution of galaxies at the corresponding redshift and magnitude range without any further selection is shown as a solid line histogram. The distribution of EROs with $(R - K) > 5.3$ is plotted as a dash-dotted line histogram; the dotted histogram shows the distribution of EROs with $(R - K) > 6$. Median stellar mass values for each distribution are indicated by an arrow with the same line style as the corresponding histogram.

and $K \leq 19.7$ account for $\sim 74\%$ of all galaxies with stellar masses in excess of $M_* > 10^{11} h^{-1} M_\odot$, in remarkably good agreement with the fraction found observationally by Conselice et al. (2008). This percentage increases with redshift.

The stellar mass distributions at higher redshift extend to larger masses than those at lower redshift. This arises because we are using a fixed apparent magnitude bin and simply sample intrinsically more luminous, and consequently more massive galaxies at high redshift.

5.3 Galaxy radii

GALFORM predicts the size of the disk and bulge components of galaxies by tracking the angular momentum of the gas which cools to make a galactic disk, and, in the case of mergers, by applying the conservation of energy and the virial theorem. In Fig. 14 we plot the predicted median half-mass radius of EROs as a function of apparent magnitude, and compare this with observational determinations of the radii of EROs from Roche et al. (2002). The shaded region in Fig. 14 shows the 90-percentile range of the model predictions. Whilst there is some overlap between the model predictions and the observational estimates at faint magnitudes, the model galaxies are on the whole too small by around a factor of two or more. It is possible that the radii of some of the observed galaxies may be overestimated, due to the ERO being associated with two galaxies which are in the

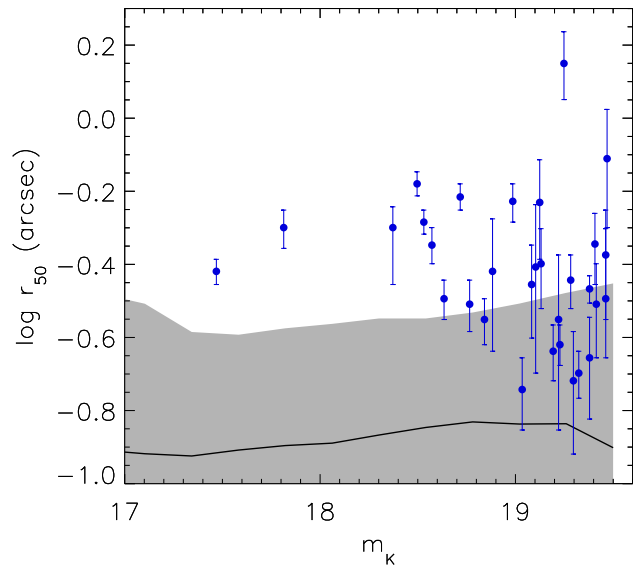


Figure 14. The median galaxy radius as a function of apparent magnitude predicted by the Bower et al. model for EROs with $(R - K) > 5$ and $K < 19.5$. The shaded region shows the 90-percentile range for predicted radii. For comparison, observational data for EROs with the same selection from Roche et al. (2002) are shown as filled circles.

process of merging, whereas the model predictions refer to the size of the merger remnant or to the sizes of the progenitor galaxies. In the Bower et al. model we find that $\sim 8\%$ of the EROs present at $z = 1.5$ experienced a merger in the preceding 1 Gyr. If this fraction of EROs are considered as close pairs in the process of merging and are assigned larger sizes (by a factor 2), then the predicted 90-percentile range would cover most of Roche et al. (2002) data points.

Almeida et al. (2007) also reported that bright, local early-type galaxies are observed to have larger radii than predicted by the model. The solution to this problem is unclear. Semi-analytical models assume that the angular momentum of the infalling gas is conserved whereas numerical simulations of disk formation show that this is not always the case (e.g. Okamoto et al. 2005). Loss of angular momentum would make the problem even worse. The self-gravity of the baryons and their pull on the dark matter halo make the disk and bulge components smaller; Almeida et al. (2007) showed that if this contraction of the dark matter halo in response to the presence of the galaxy could somehow be switched off, the correct slope is predicted for the radius-luminosity relation.

5.4 Dark halo mass

We have already shown that EROs tend to be the most massive galaxies in place at a given redshift. One might naturally expect therefore that they should be hosted by the most massive dark matter haloes present at a given epoch. In practice, the efficiency of galaxy formation tends to drop with increasing halo mass, as revealed observationally by an increase in the mass to light ratio in clusters compared with galactic haloes Eke et al. (2004), and so the trend between the luminosity of the main galaxy within a halo and halo mass could be quite weak. Furthermore, we have also

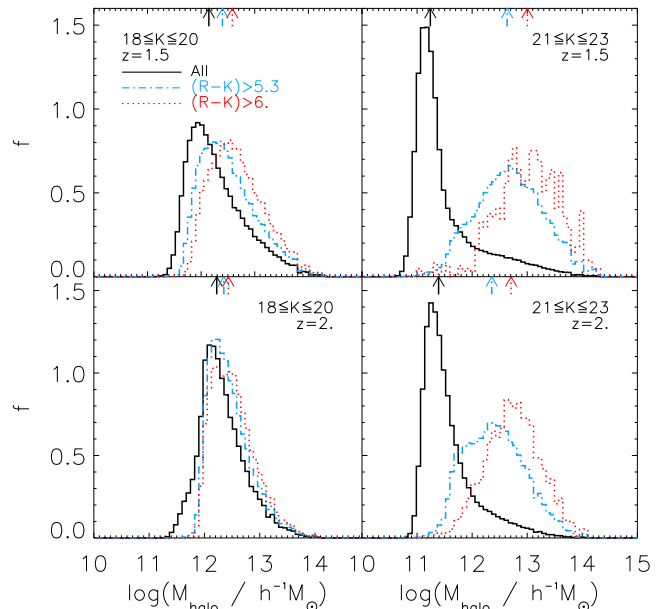


Figure 15. The distribution of host dark halo mass predicted in the Bower et al. model at redshift $z = 1.5$ (upper panels) and $z = 2$ (lower panels) for galaxies in the magnitude ranges $18 \leq K \leq 20$ (left panels) and $20 \leq K \leq 23$ (right panels). In each panel, the distribution for galaxies at the corresponding redshift and magnitude range but without any further selection is shown as a solid line histogram. The distribution of halo masses for EROs with $(R - K) > 5.3$ and with $(R - K) > 6$ are plotted with a dash-dotted and a dotted line histogram, respectively. Median halo mass values for each distribution are indicated by an arrow with the same line style as the corresponding histogram.

seen that EROs can have a wide range of luminosities and presumably can be hosted by a wide range of halo masses. Fig. 15 shows the distribution of dark halo mass for haloes which host galaxies in two ranges of K -band magnitude at $z = 1.5$ and $z = 2$. It is clear how these distributions shift to larger masses when a cut on $(R - K)$ colour is also applied. This effect is very pronounced at $z = 2$, where the median mass of haloes hosting EROs is ten times larger than that of a sample of galaxies without a colour selection. This shift in host halo mass and its dependence on the redness of the $(R - K)$ cut will have consequences for the predicted clustering of EROs. This is addressed further in Paper II.

5.5 Age of stellar populations

The formation histories of galaxies found in the deepest gravitational potential wells are shifted to earlier times compared with galaxies of the same mass found in less extreme haloes. This is a natural consequence of hierarchical structure formation (Neistein et al. 2006). The most massive haloes will tend to be found in regions with higher than average overdensity. Drawing an analogy with the spherical collapse model, the evolution of such a patch of universe will be accelerated with respect to an average density patch, with the consequence that haloes, and hence galaxies, will start to form earlier. This will lead to galaxies in massive haloes having older stellar populations. A further difference in the age of galaxies in different mass haloes will be introduced

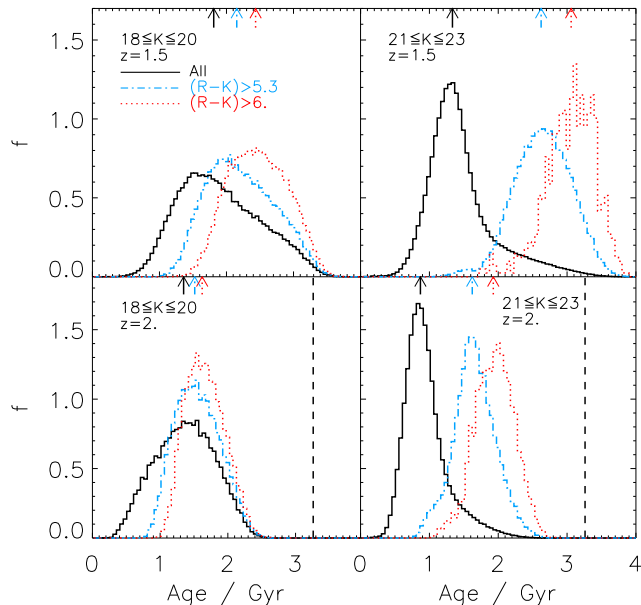


Figure 16. The distribution of the rest-frame V-band luminosity weighted stellar age predicted by the Bower et al. model at redshift $z = 1.5$ (upper panels) and $z = 2$ (lower panels) for galaxies in the magnitude ranges $18 \leq K \leq 20$ (left panels) and $20 \leq K \leq 23$ (right panels). In each panel, the distribution for galaxies at the corresponding redshift and magnitude range but without any further selection is shown as a solid line histogram. The distribution of ages for EROs with $(R - K) > 5.3$ and with $(R - K) > 6$ is plotted with a dash-dotted and a dotted line histogram, respectively. Median ages for each distribution are indicated by an arrow with the same line style as the corresponding histogram. The vertical dashed lines show the age of the Universe at $z=2$ (at $z = 1.5$ the corresponding lines lie to the right of the graph range).

if there is a physical process which acts to suppress galaxy formation preferentially in the more massive haloes.

The predicted rest-frame V-band luminosity weighted age of the stellar populations is plotted in Fig. 16. The model EROs ages have a wide distribution, with medians in the range $\sim [1.5, 3]$ Gyr.

Few observational studies have estimated the age of EROs. Using pure luminosity evolution models, Väisänen & Johansson (2004) estimated a formation redshift of around $z_f \sim 3$ for EROs. The average observed redshift of their sample is approximately $z = 1$, thus implying an age of ~ 3 Gyr. At $z = 1$, the Bower et al. model predicts that EROs with $(R - K) > 5.3$ have a median age of ~ 3 Gyr, for both the bright and faint magnitude ranges in Fig. 16, in good agreement with the estimate of Väisänen & Johansson (2004). Cimatti et al. (2002a) compared the average spectrum of quiescent EROs with stellar population synthesis models, and derived a lower limit to the age of EROs of ~ 3 Gyr. Within a similar magnitude and redshift range to those of the Cimatti et al. (2002a) sample, the Bower et al. model predicts that quiescent EROs have an average age of 3.45 Gyr, in agreement with the observational estimate. Here, as in section §4.2, we consider quiescent galaxies as those that have not experienced a recent burst of star formation.

Proceeding in a similar way to Cimatti et al. (2002a)

but considering a sample of mainly dusty starburst EROs, Schaerer et al. (2007) found ages of ~ 0.6 Gyr. The mean redshift of these EROs is $z = 1.5$. At this redshift, simulated EROs with $(R - K) > 5.3$ and $18 \leq K \leq 20$, experiencing a starburst are expected to have a mean age of 2.4 Gyr. The observed sample is composed of only 8 EROs, found behind lensing clusters. Thus, it is quite possible that the observational results are not representative of the averaged age of bursting EROs, but rather are extreme cases. More observations will be needed to reach firm conclusions about the age of bursty EROs.

6 CONCLUSIONS

In this paper we have extended the tests of the GALFORM galaxy formation code to include red galaxies at $z > 1$. Almeida et al. (2008) started this series of comparisons by presenting model predictions for the abundance of luminous red galaxies at lower redshifts, $z = 0.24$ and $z = 0.5$. The EROs we consider in this paper are not, as a whole, necessarily as intrinsically bright as luminous red galaxies. Nevertheless, the much longer look-back time to $z > 1$ poses challenges if hierarchical models are to accommodate EROs. EROs are thought to be made up of relatively old passively evolving stellar populations and dusty starbursts (e.g. McCarthy 2004). The former implies a high formation redshift for the stars and the latter suggests the presence of dust-enshrouded objects with high star formation rates.

An important feature of the calculations presented here is that they are readily connected to observations. The semi-analytical model applies simple physical recipes to determine the fate of the baryonic component of the universe. The output is the full record of galaxy mergers and the star formation history for a wide range of galaxies. The composite stellar spectrum predicted for each galaxy can then be convolved with filter transmission curves so that samples of galaxies can be constructed with the same photometric selection as the data. Moreover, by using a chemical evolution model to track the metallicity of the cold gas in galactic disks and by computing the size of the disk and bulge components, the model is able to calculate the amount of extinction experienced by starlight at any wavelength. This is a particularly important consideration given our findings regarding the nature of EROs. These galaxies seem to have a range of properties so it would be incorrect to take short cuts and assume that EROs are exclusively starburst galaxies or galaxies with little recent star formation, and then to try to use this as a proxy instead of applying the proper photometric selection of EROs.

We have tested two published models of galaxy formation, those of Baugh et al. (2005) and Bower et al. (2006). The parameters in both models were set to reproduce observations of the local galaxy population, though with different emphasis on which observations were the most important to reproduce closely. Both models enjoy successes in matching observations of the high redshift universe. The Baugh et al. model reproduces the number counts of sub-mm selected galaxies and the luminosity function of Lyman-break galaxies, whereas Bower et al. model matches the evolution of the K-band luminosity function and the inferred evolution of the stellar mass function.

The Baugh et al. model, despite the aforementioned successes at high redshift, underpredicts the counts of EROs by an order of magnitude, mirroring the predictions of earlier semi-analytical models (see e.g. Smith et al. 2002). The model predicts some passively evolving EROs (around $1/5^{\text{th}}$ of the number it should do, depending on the magnitude) but does not produce any dusty starbursts with the colour of EROs. There are dusty starbursts in the Baugh et al. model, as these are the sub-mm sources which match the observed SCUBA counts. However, there seems to be little overlap between the population of sub-mm galaxies and EROs in this model (see Smail et al. 1999, for the observational view on the connection between these two types of galaxy).

The Bower et al. model, on the other hand, gives an impressively close match to the number counts of EROs. If anything, this model predicts somewhat too many galaxies with the colours of passively evolving stellar populations at high redshift; intrinsically red galaxies dominate over dusty starbursts at all magnitudes in this model.

What does this tell us about the physics of massive galaxy formation? We experimented with the Baugh et al. model to see if its predictions could be reconciled with the observed number of EROs on changing the model parameters. An obvious place to start was the duration of starbursts. In the Baugh et al. model, starbursts have a long duration to prevent the dust from getting too hot, which would reduce the counts of sub-mm galaxies. Reducing the duration of starbursts made little difference to the predicted ERO counts, again suggesting that dusty starbursts are not the dominant population of EROs. The key seems to be that Bower et al. model gives a better match to the observed evolution of the K-band luminosity function, which means that this model puts massive galaxies in place earlier than in the Baugh et al. model. This problem has been revealed from a different point of view by Swinbank et al. (2008), who argued that the stellar masses of sub-mm galaxies are too small in Baugh et al. model. This difference between the two models arises from the different redshift dependence of the feedback processes which suppress the formation of massive galaxies and from the choice of the star formation timescale. In both models, a physical process operates to reduce the cooling rate in massive haloes. In the Baugh et al. model this is achieved by the ejection of gas in a superwind, which lowers the effective baryon fraction in massive haloes, thereby reducing the rate at which gas can cool. In the Bower et al. model, the feeding of a central supermassive black hole releases energy which stalls the cooling flow completely. The lack of a dribble of cold gas from which to form even a small amount of stars helps galaxies in the Bower et al. model to attain the colours of EROs. In Bower et al., the star formation timescale scales with the local dynamical time, whereas the scaling is independent of redshift in the Baugh et al. model. This means that a given amount of cold gas will be turned into stars more quickly at high redshift in the Bower et al. model than in the Baugh et al. model.

In the Bower et al. model, EROs are predominantly passively evolving galaxies. However, we do not find two distinct populations of objects, which suggests a transformation from a dusty starburst phase, which lasts a comparatively short time, to a longer lived quiescent phase. This is slightly at odds with observations which suggest a more equal split between passive galaxies and dusty starbursts.

Also, the redshift distribution of passive galaxies predicted by the Bower et al. model is more extended than is observed. This suggests that the star formation in massive objects may have been quenched too efficiently by the radio-mode AGN feedback. Bower et al. predict that EROs are mainly spheroid dominated, though we also find disk dominated EROs. The Bower et al. model predicts that EROs are the most massive galaxies in place at $z > 1$, in agreement with observations. The main discrepancy between the predicted properties of EROs and observations lies with the scale sizes of EROs, which are smaller than observed (see also Almeida et al. 2007).

The Bower et al. model has proven to be successful at reproducing the abundance and general properties of EROs at $z \sim 1$, and also the luminosity function of LRGs at $z = 0.24$ (Almeida et al. 2008). Both EROs and LRGs are massive, bright galaxies, dominated, at least in the model, by old stellar populations. However, the Bower et al. model does not reproduce the observed counts of sub-mm galaxies (Swinbank et al. 2008), which are also massive galaxies, with stellar mass $M > 10^{11} M_{\odot}$ at $z \sim 2$, experiencing active star formation. On the other hand, the Baugh et al. model does reproduce the counts and redshift distribution of sub-mm galaxies, but does less well at matching the abundance of red galaxies at $z < 1$. In a later paper in this series, we will investigate the nature of the objects selected by different colour and magnitude criteria. The semi-analytical model is ideally suited to connecting galaxies identified at high redshift with their local, $z = 0$ counterparts. We will address the issue of what fraction of today's galaxies had a progenitor which passed the criteria to be identified as a red galaxy and we will determine what fraction of the present day stellar mass was already in place by this epoch.

This is the first paper in a series which examines the properties and nature of red galaxies in hierarchical models. Here we have presented predictions for the abundance and redshift distribution of EROs, along with some basic properties, such as stellar mass and host halo mass. In the second paper we present predictions for the clustering of EROs and in the third we compare different colour cuts used to select red galaxies and compare the properties of their present day descendants.

ACKNOWLEDGMENTS

We thank S. Foucaud, C. Simpson and I. Smail for providing their measured EROs number counts in a table format. We also acknowledge F. J. Castander, J. Helly, A. Benson, R. Malbon and M. Swinbank for discussions and comments. We thank the referee for a helpful report. VGP acknowledges support from CSIC/IEEC, the Spanish Ministerio de Ciencia y Tecnología and travel support from a Royal Society International Joint Project grant. CMB was supported by the Royal Society. CGL is supported in part by a grant from the Science and Technology Facilities Council. CA gratefully acknowledges a scholarship from the FCT, Portugal.

REFERENCES

- Abraham R. G. et al., 2007, ApJ, 669, 184
- Almeida C., Baugh C. M., Lacey C. G., 2007, MNRAS, 376, 1711

- Almeida C., Baugh C. M., Wake D. A., Lacey C. G., Benson A. J., Bower R. G., Pimbblet K., 2008, *MNRAS*, 386, 2145
- Baugh C. M., 2006, *Reports of Progress in Physics*, 69, 3101
- Baugh C. M., Cole S., Frenk C. S., 1996, *MNRAS*, 283, 1361
- Baugh C. M., Efstathiou G., 1993, *MNRAS*, 265, 145
- Baugh C. M., Lacey C. G., Frenk C. S., Granato G. L., Silva L., Bressan A., Benson A. J., Cole S., 2005, *MNRAS*, 356, 1191
- Benson A. J., Bower R. G., Frenk C. S., Lacey C. G., Baugh C. M., Cole S., 2003, *ApJ*, 599, 38
- Bergström S., Wiklund T., 2004, *A&A*, 414, 95
- Bershady M. A., Lowenthal J. D., Koo D. C., 1998, *ApJ*, 505, 50
- Bower R. G., Benson A. J., Malbon R., Helly J. C., Frenk C. S., Baugh C. M., Cole S., Lacey C. G., 2006, *MNRAS*, 370, 645
- Brown M. J. I., Jannuzi B. T., Dey A., Tiede G. P., 2005, *ApJ*, 621, 41
- Calzetti D., Armus L., Bohlin R. C., Kinney A. L., Koornneef J., Storchi-Bergmann T., 2000, *ApJ*, 533, 682
- Cattaneo A., Dekel A., Devriendt J., Guiderdoni B., Blaizot J., 2006, *MNRAS*, 370, 1651
- Cimatti A. et al., 2002a, *A&A*, 381, L68
- , 2002b, *A&A*, 391, L1
- , 2003, *A&A*, 412, L1
- , 2004, *Nature*, 430, 184
- Cirasuolo M. et al., 2007, *MNRAS*, 380, 585
- Cole S., Lacey C. G., Baugh C. M., Frenk C. S., 2000, *MNRAS*, 319, 168
- Conselice C. J., Bundy K., U V., Eisenhardt P., Lotz J., Newman J., 2008, *MNRAS*, 383, 1366
- Cowie L. L., Barger A. J., Hu E. M., Capak P., Songaila A., 2004, *AJ*, 127, 3137
- Cowie L. L., Songaila A., Hu E. M., Cohen J. G., 1996, *AJ*, 112, 839
- Croton D. J. et al., 2006, *MNRAS*, 365, 11
- Daddi E., Cimatti A., Renzini A., 2000, *A&A*, 362, L45
- Daddi E., Cimatti A., Renzini A., Fontana A., Mignoli M., Pozzetti L., Tozzi P., Zamorani G., 2004, *ApJ*, 617, 746
- de Lucia G., Springel V., White S. D. M., Croton D., Kauffmann G., 2006, *MNRAS*, 366, 499
- de Lucia G., Blaizot J., 2007, *MNRAS*, 375, 2
- Djorgovski S. et al., 1995, *ApJL*, 438, L13
- Doherty M., Bunker A. J., Ellis R. S., McCarthy P. J., 2005, *MNRAS*, 361, 525
- Efstathiou G., Bernstein G., Tyson J. A., Katz N., Guhathakurta P., 1991, *ApJL*, 380, L47
- Eggen O. J., Lynden-Bell D., Sandage A. R., 1962, *ApJ*, 136, 748
- Eisenstein D. J., et al., 2001, *AJ*, 122, 2267
- Eke V. R. et al., 2004, *MNRAS*, 355, 769
- Elston R., Rieke G. H., Rieke M. J., 1988, *ApJL*, 331, L77
- Ferrara A., Bianchi S., Cimatti A., Giovanardi C., 1999, *ApJS*, 123, 437
- Firth A. E. et al., 2002, *MNRAS*, 332, 617
- Font A. S. et al., 2008, *MNRAS*, 389, 1619
- Fontana A. et al., 2004, *A&A*, 424, 23
- Fontanot F., Monaco P., Silva L., Grazian A., 2007, *MNRAS*, 382, 903
- Frith W. J., Metcalfe N., Shanks T., 2006, *MNRAS*, 371, 1601
- Gardner J. P., Cowie L. L., Wainscoat R. J., 1993, *ApJL*, 415, L9
- Gardner J. P., Sharples R. M., Carrasco B. E., Frenk C. S., 1996, *MNRAS*, 282, L1
- Glazebrook K., Ellis R., Colless M., Broadhurst T., Allington-Smith J., Tanvir N., 1995a, *MNRAS*, 273, 157
- Glazebrook K. et al., 2004, *Nature*, 430, 181
- Glazebrook K., Peacock J. A., Miller L., Collins C. A., 1995b, *MNRAS*, 275, 169
- Granato G. L., De Zotti G., Silva L., Bressan A., Danese L., 2004, *ApJ*, 600, 580
- Granato G. L., Lacey C. G., Silva L., Bressan A., Baugh C. M., Cole S., Frenk C. S., 2000, *ApJ*, 542, 710
- Helly J. C., Cole S., Frenk C. S., Baugh C. M., Benson A., Lacey C., Pearce F. R., 2003, *MNRAS*, 338, 913
- Hopkins P. F., Hernquist L., Cox T. J., Robertson B., Springel V., 2006, *ApJS*, 163, 50
- Huang J.-S., Cowie L. L., Gardner J. P., Hu E. M., Songaila A., Wainscoat R. J., 1997, *ApJ*, 476, 12
- Huang J.-S. et al., 2001, *A&A*, 368, 787
- Kang X., Jing Y. P., Silk J., 2006, *ApJ*, 648, 820
- Kennicutt Jr. R. C., 1983, *ApJ*, 272, 54
- Kitzbichler M. G., White S. D. M., 2006, *MNRAS*, 366, 858
- , 2007, *MNRAS*, 376, 2
- Kochanek C. S. et al., 2001, *ApJ*, 560, 566
- Kong X. et al., 2006, *ApJ*, 638, 72
- Kümmel M. W., Wagner S. J., 2001, *A&A*, 370, 384
- Lacey C. G., Baugh C. M., Frenk C. S., Silva L., Granato G. L., Bressan A., 2008, *MNRAS*, 385, 1155
- Lagos C. D. P., Cora S. A., Padilla N. D., 2008, *MNRAS*, 388, 587
- Lawrence A. et al., 2007, *MNRAS*, 379, 1599
- Le Delliou M., Lacey C., Baugh C. M., Guiderdoni B., Bacon R., Courtois H., Sousbie T., Morris S.L., 2005, *MNRAS*, 357, L11
- Le Delliou M., Lacey C., Baugh C. M., Morris S.L., 2006, *MNRAS*, 365, 712
- Maihara T. et al., 2001, *PASJ*, 53, 25
- Malbon R. K., Baugh C. M., Frenk C. S., Lacey C. G., 2007, *MNRAS*, 382, 1394
- Mamon G. A., 1998, in *Wide Field Surveys in Cosmology*, Colombi S., Mellier Y., Raban B., eds., pp. 323–+
- Mannucci F., Pozzetti L., Thompson D., Oliva E., Baffa C., Comoretto G., Gennari S., Lisi F., 2002, *MNRAS*, 329, L57
- Martini P., 2001, *AJ*, 121, 598
- McCarthy I. G., Frenk C. S., Font A. S., Lacey C. G., Bower R. G., Mitchell N. L., Balogh M. L., Theuns T., 2008, *MNRAS*, 383, 593
- McCarthy P. J., 2004, *ARA&A*, 42, 477
- McCarthy P. J. et al., 2001, *ApJL*, 560, L131
- McCracken H. J., Metcalfe N., Shanks T., Campos A., Gardner J. P., Fong R., 2000, *MNRAS*, 311, 707
- McLeod B. A., Bernstein G. M., Rieke M. J., Tollestrup E. V., Fazio G. G., 1995, *ApJS*, 96, 117
- Menci N., Fontana A., Giallongo E., Grazian A., Salimbeni S., 2006, *ApJ*, 647, 753
- Metcalfe N., Shanks T., Campos A., McCracken H. J., Fong R., 2001, *MNRAS*, 323, 795
- Miyazaki M. et al., 2003, *PASJ*, 55, 1079

- Mo H. J., White S. D. M., 2002, MNRAS, 336, 112
- Mobasher B., Ellis R. S., Sharples R. M., 1986, MNRAS, 223, 11
- Monaco P., Fontanot F., Taffoni G., 2007, MNRAS, 375, 1189
- Moriondo G., Cimatti A., Daddi E., 2000, A&A, 364, 26
- Moustakas L. A., Davis M., Graham J. R., Silk J., Peterson B. A., Yoshii Y., 1997, ApJ, 475, 445
- Moustakas L. A. et al., 2004, ApJL, 600, L131
- Nagamine K., Cen R., Hernquist L., Ostriker J. P., Springel V., 2005, ApJ, 627, 608
- Nagashima M., Lacey C. G., Okamoto T., Baugh C. M., Frenk C. S., Cole S., 2005, MNRAS, 363, L31
- Neistein E., van den Bosch F. C., Dekel A., 2006, MNRAS, 372, 933
- Norberg P. et al., 2002, MNRAS, 332, 827
- Okamoto T., Eke V. R., Frenk C. S., Jenkins A., 2005, MNRAS, 363, 1299
- Orsi A., Lacey C. G., Baugh C. M., Infante L., 2008, MNRAS, in press. (arXiv:0807.3447)
- Parkinson H., Cole S., Helly J., 2008, MNRAS, 383, 557
- Pozzetti L., Mannucci F., 2000, MNRAS, 317, L17
- Roche N. D., Almaini O., Dunlop J., Ivison R. J., Willott C. J., 2002, MNRAS, 337, 1282
- Salpeter E. E., 1955, ApJ, 121, 161
- Sánchez A. G., Baugh C. M., Percival W. J., Peacock J. A., Padilla N. D., Cole S., Frenk C. S., Norberg P., 2006, MNRAS, 366, 189
- Saracco P., Giallongo E., Cristiani S., D'Odorico S., Fontana A., Iovino A., Poli F., Vanzella E., 2001, A&A, 375, 1
- Saracco P., Iovino A., Garilli B., Maccagni D., Chincarini G., 1997, AJ, 114, 887
- Schaerer D. et al., 2007, A&A, 476, 97
- Sijacki D., Springel V., di Matteo, T., Hernquist L., 2007, MNRAS, 380, 877
- Silk J., Rees M. J., 1998, A&A, 331, L1
- Silva L., Granato G. L., Bressan A., Danese L., 1998, ApJ, 509, 103
- Simien F., de Vaucouleurs G., 1986, ApJ, 302, 564
- Simpson C. et al., 2006, MNRAS, 373, L21
- Smail I., Ivison R. J., Kneib J.-P., Cowie L. L., Blain A. W., Barger A. J., Owen F. N., Morrison G., 1999, MNRAS, 308, 1061
- Smail I., Owen F. N., Morrison G. E., Keel W. C., Ivison R. J., Ledlow M. J., 2002, ApJ, 581, 844
- Smith G. P., Smail I., Kneib J.-P., Davis C. J., Takamiya M., Ebeling H., Czoske O., 2002, MNRAS, 333, L16
- Soifer B. T. et al., 1994, ApJL, 420, L1
- Somerville R. S., Lee K., Ferguson H. C., Gardner J. P., Moustakas L. A., Giavalisco M., 2004, ApJL, 600, L171
- Somerville R. S., Hopkins P. F., Cox T. J., Robertson B. E., Hernquist, L., 2008, MNRAS, 391, 481
- Songaila A. Cowie L. L., Lilly S. J., 1990, ApJ, 348, 371
- Springel V. et al., 2005, Nature, 435, 629
- Swinbank A. M. et al., 2008, MNRAS, 391, 420
- Szokoly G. P., Subbarao M. U., Connolly A. J., Mobasher B., 1998, ApJ, 492, 452
- Thompson D. et al., 1999, ApJ, 523, 100
- Väisänen P., Johansson P. H., 2004, A&A, 421, 821
- Väisänen P., Tollestrup E. V., Willner S. P., Cohen M., 2000, ApJ, 540, 593
- Vandame B. et al., 2001, ArXiv Astrophysics e-prints
- Weinmann S. M., van den Bosch F. C., Yang X., Mo H. J., Croton D. J., Moore B., 2006, MNRAS, 372, 1161